
Article:
Kirk, V and Rucklidge, AM orcid.org/0000-0003-2985-0976 (2008) The effect of symmetry breaking on the dynamics near a structurally stable heteroclinic cycle between equilibria and a periodic orbit. Dynamical Systems, 23 (1). pp. 43-74. ISSN 1468-9367

https://doi.org/10.1080/14689360701709088

Dynamical Systems: An International Journal
Vol. 00, No. 00, June 2007, 1–43

The effect of symmetry breaking on the dynamics near a structurally stable heteroclinic cycle between equilibria and a periodic orbit

Vivien Kirk, Department of Mathematics, University of Auckland,
Private Bag 92019, Auckland, New Zealand
Alastair M. Rucklidge, Department of Applied Mathematics, University of Leeds,
Leeds LS2 9JT, UK

(May 7, 2008)

The effect of small forced symmetry breaking on the dynamics near a structurally stable heteroclinic cycle connecting two equilibria and a periodic orbit is investigated. This type of system is known to exhibit complicated, possibly chaotic dynamics including irregular switching of sign of various phase space variables, but details of the mechanisms underlying the complicated dynamics have not previously been investigated. We identify global bifurcations that induce the onset of chaotic dynamics and switching near a heteroclinic cycle of this type, and by construction and analysis of approximate return maps, locate the global bifurcations in parameter space. We find there is a threshold in the size of certain symmetry-breaking terms below which there can be no persistent switching. Our results are illustrated by a numerical example.

1 Introduction

It is well-established that the presence of symmetries in dynamical systems can result in the existence of heteroclinic cycles that are structurally stable with respect to symmetric perturbations [1, 2]. By *heteroclinic cycle* we mean a collection of two or more flow invariant sets $\{\xi_1, \ldots, \xi_n\}$ of some system of ordinary differential equations together with a set of heteroclinic connections $\{\gamma_1(t), \ldots, \gamma_n(t)\}$, where $\gamma_j(t) \to \xi_j$ as $t \to -\infty$ and $\gamma_j(t) \to \xi_{j+1}$ as $t \to +\infty$, and where $\xi_{n+1} \equiv \xi_1$. In many studies, all the ξ_i are equilibria, but in this

V.Kirk@auckland.ac.nz
A.M.Rucklidge@leeds.ac.uk

paper we explicitly consider the case that one of the ξ_i is a periodic orbit. The connections γ_i may be isolated, or there may be a continuum of connections from ξ_i to ξ_{i+1} for one or more i.

There is a large literature on structurally stable heteroclinic cycles (SSHC), including work establishing conditions for the existence and asymptotic stability of heteroclinic cycles [3–5], examination of the dynamics near heteroclinic cycles and networks of heteroclinic cycles [6–9], and unfolding of bifurcations of heteroclinic cycles [10–12]. SSHC arise naturally in mathematical models of physical systems with symmetry or near-symmetry [13–16]. In these models, the physical system is idealised as having perfect symmetry, leading to the existence of invariant subspaces in the model and thus to the robustness of heteroclinic cycles with respect to symmetric perturbations. It is natural to ask how much of the dynamics observed in symmetric models persists under non-symmetric perturbations. Some effects of small symmetry-breaking have been documented [17–20], and aspects of the related question of how much of the dynamics persists under the inclusion of small noise have also been considered [21, 22], but details are likely to vary greatly between different examples. A few cases of experimental observation of near-heteroclinic cycles have been reported, most recently in [23], but see also the references therein. In these cases, experimental noise and small symmetry-breaking effects prevent exact heteroclinic cycles from occurring, but there is clear evidence for near-heteroclinic structures in certain regimes.

Our interest in the particular set-up explored in this paper is motivated by [20], which makes the observation that the addition of small symmetry-breaking terms to a system containing a heteroclinic cycle connecting two equilibria and a periodic orbit (as well as symmetric copies of the cycle) results in seemingly chaotic dynamics, with orbits passing near the various equilibria in the system repeatedly but in an irregular pattern, as illustrated in figure 1. A main point of [20] was to show that repeated switching of orbits in this manner could arise in a simple four-dimensional, nearly symmetric model, but the specific mechanisms underlying the complicated dynamics were not explored in detail.

In this paper, we examine a generalisation of the situation from [20], focusing on the structure and origin of chaotic dynamics in the system and on how switching dynamics is induced. Here and elsewhere in the paper, *switching*

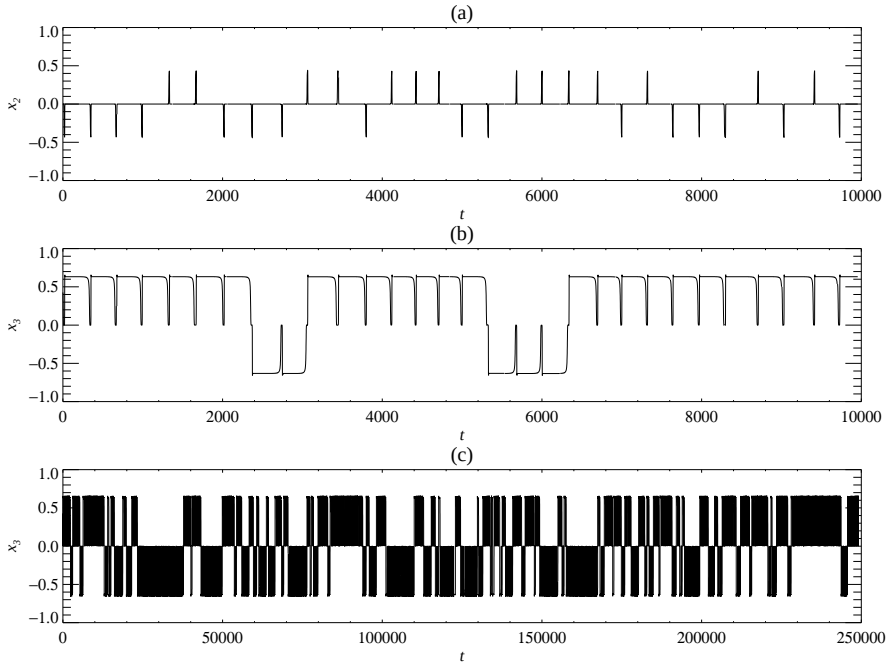

Figure 1. Irregular switching in the time series of a dynamo model studied in [20, figure 1]. Panels (a) and (b) show the evolution of different coordinates of the same trajectory, and panel (c) shows the same coordinate as in (b) over a longer time interval.

refers to the itinerary that an orbit follows under the dynamics. Specifically, in the fully symmetric version of our system there is a heteroclinic network consisting of four symmetric copies of the basic heteroclinic cycle. Invariance of various subspaces ensures that an orbit may make repeated passes near only one cycle. Once the symmetries are broken, however, an orbit may *switch*, i.e., make traversals near more than one of the original cycles (although, of course, the cycles themselves may not persist when the symmetry is broken).

A main result of this paper is that in the case of small symmetry breaking, switching in one variable occurs when a complicated attractor arising from the presence of transverse homoclinic orbits of a periodic orbit crosses the stable manifold of one of the equilibria in the system. The existence of the transverse homoclinic orbits depends on a broken rotation symmetry, while the proximity of the attractor to the stable manifold of the equilibrium is caused by a broken reflection symmetry. Switching in a second variable results from the interaction between broken reflection symmetry and complicated dynamics associated with a heteroclinic bifurcation between the equilibria. Thus, switching

results from the right combination of a global bifurcation and small symmetry breaking.

A second significant result of this paper is the observation that there is a threshold for the size of symmetry breaking below which persistent switching cannot occur. More precisely, the existence of the heteroclinic cycle requires three separate symmetries to allow structurally stable connections within three invariant subspaces. We control the degree to which the three symmetries are broken by three small parameters, ϵ_1, ϵ_2 and ϵ_3; ϵ_1 controls the degree to which the periodic orbit in the cycle deviates from a perfect circle, while ϵ_2 and ϵ_3 break reflection symmetries. For fixed small ϵ_2 and ϵ_3, we find that there is a threshold in ϵ_1 for persistent switching to occur. For sufficiently small ϵ_1, there may be a single switch from one part of phase space to another, but it is only for ϵ_1 beyond the threshold value that an orbit can repeatedly visit different parts of the phase space. We find that it is possible to get sustained switching in one or other or both of the variables associated with the reflection symmetries, and that the threshold values of ϵ_1 are different for switching in the two variables. The threshold does not go to zero as ϵ_2 and ϵ_3 go to zero.

Sustained switching of orbits near heteroclinic cycles and networks has been observed in a number of other settings. Clune and Knobloch [24] describe an example in which there are two symmetrically related copies of a non-asymptotically stable heteroclinic cycle, with nearby orbits making repeated passes near each cycle; no mechanism for the switching is suggested in this paper. Aguiar et al. [8] find switching near a hybrid heteroclinic network formed from transverse heteroclinic connections between equilibria and connections that are robust because of symmetry; switching seems to result from the folding and stretching caused by passage near the transversal heteroclinic connections and by mixing near an equilibrium solution with complex eigenvalues. Kirk et al. [25] have an example of switching near a heteroclinic network that has no transversal connections; the switching is caused entirely by passage near an equilibrium with complex eigenvalues. Postlethwaite and Dawes [9] describe a variant of switching near a heteroclinic network in which each cycle in the network is unstable along a direction transverse to the cycle; orbits visit cycles in the network in a fixed order (being pushed away from each cycle in the transverse direction, which also happens to be the contracting direction for the next cycle) but the number of traversals of each cycle before switch-

ing to the next cycle can be constant or irregular. Ashwin et al. [26] describe switching associated with a stuck-on heteroclinic cycle between two invariant subspaces; here the switching is caused by a nonlinear mechanism that chooses between the different possibilities in a manner that is well modelled by a random process. Switching can also be induced by adding noise to a structurally stable heteroclinic network [22]; noise sensitive switching has been observed by [27, 28]. None of these examples explicitly considers symmetry breaking as a mechanism for switching.

We adopt a standard approach to analysis of the system of interest, i.e., we set up a simple symmetric model in which there exists a heteroclinic cycle connecting two equilibria and a periodic orbit (Section 2), construct a return map that approximates the dynamics near such a cycle, and then add generic symmetry breaking terms to the return map (Section 3, with details in the Appendix). Analysis of the return map is fruitful in cases where partial symmetry is retained, and allows us to prove the existence and asymptotic stability of periodic orbits, quasiperiodic solutions or heteroclinic cycles in various cases (Sections 4.1–4.3). In the completely asymmetric case, the return map is intractable, but we are able to make predictions about the dynamics by assuming there is a generic unfolding of the partially symmetric cases (Section 4.4). The example discussed in Section 5 confirms and illustrates the analysis. Some conclusions are presented in Section 6.

A complicating factor in the analysis presented in this paper is that the unstable manifolds of one pair of equilibria and of the periodic orbit are two-dimensional, and there are continua of heteroclinic connections along some parts of the cycle in the fully symmetric case. Linearising about a single heteroclinic connection is not appropriate, and the usual method of analysis needs to be adapted to keep track of orbits in a neighbourhood of all the connections. Our approach is similar to that taken in [7, 25, 29]. We note that our analysis need not consider the issue of which connection from a continuum is selected by the dynamics (as investigated in, for instance, [7, 26, 30, 31]) since in our case breaking of the symmetries forces a discrete set of transversal connections to be selected from each continuum. Note also that some results about the dynamics near a heteroclinic cycle connecting an equilibrium and a periodic orbit in a generic (i.e., non-symmetric) setting are described in [32, 33], but the phenomena described in those papers will not be seen for small symmetry

breaking in our setting, and is not the focus of our interest here.

2 Description of the problem

We consider a system of ordinary differential equations $\dot{\mathbf{x}} = \mathbf{f}(\mathbf{x})$ where $\mathbf{f} : \mathbb{R}^4 \to \mathbb{R}^4$, and $\mathbf{x} = (x_1, y_1, x_2, x_3) \in \mathbb{R}^4$. It is sometimes convenient to use polar coordinates (r_1, θ_1) such that $z_1 \equiv x_1 + \mathrm{i}\, y_1 \equiv r_1 \mathrm{e}^{\mathrm{i}\theta_1}$. Initially, we assume the system is equivariant with respect to the action of a rotation and two reflections: $\kappa_i(\mathbf{f}(\mathbf{x})) = \mathbf{f}(\kappa_i(\mathbf{x}))$, $i = 1, 2, 3$, where

$$\kappa_1 \colon (z_1, x_2, x_3) \to (z_1 \mathrm{e}^{\mathrm{i}\phi}, x_2, x_3),$$
$$\kappa_2 \colon (z_1, x_2, x_3) \to (z_1, -x_2, x_3),$$
$$\kappa_3 \colon (z_1, x_2, x_3) \to (z_1, x_2, -x_3),$$

with $0 \le \phi < 2\pi$. These symmetries generate the group $S^1 \times Z_2 \times Z_2$, and their presence ensures the existence of some dynamically invariant subspaces. We make the following assumptions about the dynamics in the subspaces, as illustrated in figure 2:

- There exists a hyperbolic periodic orbit P in the invariant plane $x_2 = x_3 = 0$. Within this plane, the periodic orbit is a sink.
- There exist hyperbolic, symmetry-related pairs of equilibria $\pm E_2$ and $\pm E_3$ on the invariant lines $z_1 = 0$, $x_3 = 0$ and $z_1 = 0$, $x_2 = 0$ respectively. Within these lines, the equilibria are sinks.
- Within the invariant subspace $x_3 = 0$, P is a saddle and $\pm E_2$ are sinks, and there are two-dimensional manifolds of heteroclinic connections from P to $\pm E_2$ (figure 2a).
- Within the invariant subspace $z_1 = 0$, $\pm E_2$ are saddles and $\pm E_3$ are sinks, and there are one-dimensional heteroclinic connections from $+E_2$ to $\pm E_3$, and from $-E_2$ to $\pm E_3$ (figure 2b).
- Within the invariant subspace $x_2 = 0$, $\pm E_3$ are saddles and P is a sink, and there are two-dimensional manifolds of heteroclinic connections from $\pm E_3$ to P (figure 2c).

In the presence of the rotation symmetry κ_1, the coordinate θ_1 decouples from the other coordinates, leaving an equivalent three-dimensional system

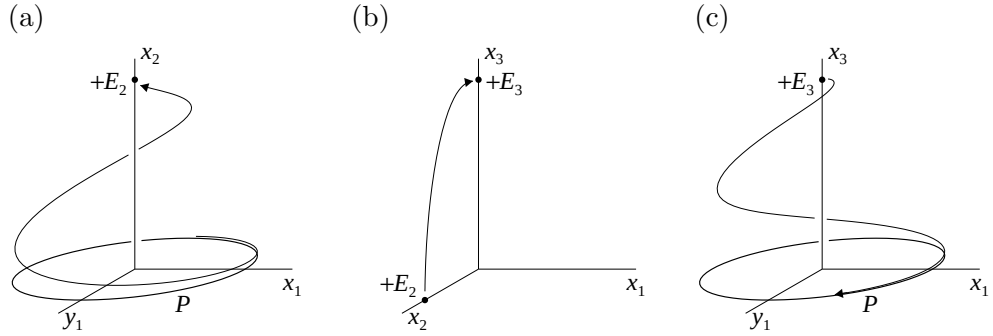

Figure 2. The heteroclinic cycle for the fully symmetric system. (a) One of the connections in the $x_3 = 0$ subspace, from the periodic orbit P to the equilibrium point $+E_2$; (b) the single connection in the $x_1 = y_1 = 0$ subspace, between the equilibria $+E_2$ and $+E_3$; (c) one of the connections in the $x_2 = 0$ subspace, from $+E_3$ to P.

containing a SSHC connecting three saddle-type equilibria. This cycle may be asymptotically stable, depending on the eigenvalues at the three equilibria [4]. The behaviour of trajectories near such a heteroclinic cycle is well understood, with a typical orbit passing near each of the equilibria in a cyclic manner, spending ever increasing periods of time near each equilibrium. The dynamics in the fully symmetric, four-dimensional problem therefore has analogous behaviour: trajectories cycle between two equilibria and a periodic orbit, with the time spent near each equilibrium or the periodic orbit increasing with each subsequent traversal of the cycle [20]. Moving to four dimensions does more than replace one pair of equilibria by a periodic orbit: it also introduces dynamical features that will be important once symmetry is broken. In particular, as can be seen in figure 2, $\pm E_2$ and $\pm E_3$ are saddle-foci in the four-dimensional problem, and P and $\pm E_3$ have two-dimensional unstable manifolds.

A detailed analysis of the effect on the dynamics of small symmetry breaking is performed in the following sections; here we describe some geometric effects. Since $\pm E_2$, $\pm E_3$ and P are assumed to be hyperbolic in the fully symmetric case, they persist and are hyperbolic when sufficiently small symmetry breaking terms are added. However, $+E_2$ and $-E_2$ will generically move off the x_2-axis and will no longer be related to each other by symmetry. Generic symmetry breaking will have an analogous effect on $+E_3$ and $-E_3$, and will also break the circular symmetry of P and move it off the plane $x_2 = x_3 = 0$.

Sufficiently small symmetry breaking will not change the dimensions of the stable and unstable manifolds of $\pm E_2$, $\pm E_3$ and P, but it will destroy the

invariant subspaces, and the heteroclinic connections that existed in the subspaces will either cease to exist or change their nature. We consider the geometric effect of symmetry breaking on each of the former heteroclinic connections in turn.

The heteroclinic connections from $\pm E_2$ to $\pm E_3$ require the coincidence in $\mathbb{R}^4$ of one-dimensional and two-dimensional manifolds; these connections will be destroyed by a generic symmetry-breaking perturbation.

The heteroclinic connections from $\pm E_3$ to P occur when the two-dimensional unstable manifolds of $\pm E_3$ intersect the three-dimensional stable manifold of P. Depending on the perturbation, we generically expect to see either transversal intersections between these manifolds (in which case there are, for example, at least two robust heteroclinic connections from $+E_3$ to P) or no intersections of the manifolds. The special case where the manifolds are tangent can also occur in a codimension-one way. In the case of transversal intersections of manifolds, we might expect to see heteroclinic tangles and the associated complicated dynamics, depending on whether the dynamics elsewhere in the phase space permits reinjection of trajectories into the neighbourhood of the transversal intersections.

The heteroclinic connections from P to $\pm E_2$ occur when the two-dimensional unstable manifold of P intersects the three-dimensional stable manifolds of $\pm E_2$. There is a clear analogy with the case of connections from $\pm E_3$ to P and the comments about that case apply equally here.

While small symmetry-breaking terms generically destroy the heteroclinic cycle, there will still be an attractor lying close to the original heteroclinic cycle (Melbourne [17] shows this in a closely related case). We show below that the form of this attractor (e.g., periodic, quasiperiodic, chaotic) depends on the nature of the symmetry-breaking perturbations included. In the fully symmetric case, the invariant subspaces defined by $x_2 = 0$ and by $x_3 = 0$ restrict each trajectory to one quarter of the phase space, but once the reflection symmetries are broken, a single trajectory may explore more of the phase space. We are interested in determining the circumstances under which trajectories exhibit switching, i.e., make passages near two or more quarters of the original heteroclinic attractor.

3 Construction of return maps

We construct and analyse a return map that approximates the dynamics near the cycle. The idea is to define local coordinates and cross-sections near $\pm E_2$, $\pm E_3$ and P, then determine local maps valid in a neighbourhood of each of $\pm E_2$, $\pm E_3$ and P, and global maps valid in a neighbourhood of each heteroclinic connection. Composing the local and global maps yields the desired return map. Different forms for the return map are obtained depending on which of the symmetries are broken. In this section we list the different cases, but details of map construction are left to the Appendix. The techniques used are, for the most part, standard, although modifications are required to allow for the existence of continua of heteroclinic connections along some parts of the cycle in the fully symmetric case.

Throughout, we use a small parameter h to control the size of the local neighbourhoods ($h \ll 1$), and small parameters ϵ_1, ϵ_2, ϵ_3 to control the extent to which the symmetries κ_1, κ_2, κ_3 are broken. It turns out to be convenient to define the return map on a cross-section near $+E_3$. Using local coordinates $(r_1, \theta_1, x_2, \xi_3)$ near $+E_3$, where coordinates are chosen so that $+E_3$ is at the origin and so that the eigenvectors of the linearised flow align with the coordinate axes in the manner described in the Appendix, we define a cross-section

$$H_3^{\text{in}} = \{(r_1, \theta_1, x_2, \xi_3) : 0 \le r_1 \le h, |x_2| = h, |\xi_3| \le h\}$$

and then compute the return map, $R : H_3^{\text{in}} \to H_3^{\text{in}}$. The same cross-section works equally well near $-E_3$ and the maps R we compute in fact approximate the dynamics near any of the four possible paths from $\pm E_3$ to $\pm E_3$. See the Appendix for details.

Since we are interested in trajectories that switch between positive and negative values of x_2 and x_3, we introduce the notation $\pm_2$ and $\pm_3$ to indicate whether a trajectory visits $+E_2$ or $-E_2$, and $+E_3$ or $-E_3$. In particular, the trajectory starts at one of four possible sections specified by H_3^{in}, and we use $\pm_2$ to specify whether $x_2 = +h$ or $x_2 = -h$ (implying that the trajectory recently visited $+E_2$ or $-E_2$). We use $\pm_3$ to specify whether the trajectory is close to $+E_3$ or $-E_3$. When the trajectory next returns to H_3^{in}, we will be interested in whether it visited $+E_2$ or $-E_2$ en route, and whether it returns to $+E_3$ or $-E_3$.

First, in the case with full symmetry ($\epsilon_1 = \epsilon_2 = \epsilon_3 = 0$), we have:

$$R(r_1, \theta_1, x_2 = \pm_2 h, \xi_3) = \Big(\tilde{r}_1 = A r_1^{\delta}, \tilde{\theta}_1 = \theta_1 + \Phi - Q \ln r_1, \\ \tilde{x}_2 = x_2, \tilde{\xi}_3 = B_2\Big), \tag{1}$$

where $A > 0$ and Φ are constants, $\delta = \delta_1\delta_2\delta_3$, $Q = (e_1e_2 + e_2c_3 + c_3c_1)/e_1e_2e_3$, and the constants δ_i, e_i and c_i are defined in the Appendix. If $x_3 > 0$ initially, the trajectory returns to $+E_3$ after visiting $\pm_2 E_2$; if $x_3 < 0$ initially, the trajectory returns to $-E_3$.

Second, breaking the κ_2 and κ_3 symmetries ($\epsilon_1 = 0$, $\epsilon_2 \neq 0$, $\epsilon_3 \neq 0$) we have:

$$\begin{aligned} R(r_1, \theta_1, x_2 = \pm_2 h, \xi_3) = \Big(&\tilde{r}_1 = A_2 \Big| \epsilon_3 \pm_3 A_1 \big| \epsilon_2 \pm_2 A_3 r_1^{\delta_3} \big|^{\delta_1} \Big|^{\delta_2}, \\ &\tilde{\theta}_1 = \theta_1 + \Phi_1 + \Phi_2 + \Phi_3 - \frac{1}{e_3} \ln r_1 \\ &\quad - \frac{1}{e_1} \ln \left| \epsilon_2 \pm_2 A_3 r_1^{\delta_3} \right| \\ &\quad - \frac{1}{e_2} \ln \Big| \epsilon_3 \pm_3 A_1 \big| \epsilon_2 \pm_2 A_3 r_1^{\delta_3} \big|^{\delta_1} \Big|, \\ &\tilde{x}_2 = \operatorname{sgn}\left(\epsilon_2 \pm_2 A_3 r_1^{\delta_3} \right) h, \tilde{\xi}_3 = B_2 \Big). \end{aligned} \tag{2}$$

The trajectory visits $+E_2$ or $-E_2$ en route according to the sign of $\epsilon_2 \pm_2 A_3 r_1^{\delta_3}$, and it returns to $+E_3$ or $-E_3$ according to the sign of $\epsilon_3 \pm_3 A_1 \big| \epsilon_2 \pm_2 A_3 r_1^{\delta_3} \big|^{\delta_1}$.

Third, if we break the κ_1 symmetry but preserve κ_2 and κ_3 ($\epsilon_1 \neq 0$, $\epsilon_2 = \epsilon_3 = 0$) we have:

$$R(r_1, \theta_1, x_2 = \pm_2 h, \xi_3) = \Big(\tilde{x}_1 = \epsilon_1 a_{\mathrm{r}} + A_2 |\hat{x}_3|^{\delta_2} \cos\hat{\theta}_1, \\ \tilde{y}_1 = \epsilon_1 a_{\mathrm{i}} + A_2 |\hat{x}_3|^{\delta_2} \sin\hat{\theta}_1, \\ \tilde{x}_2 = \operatorname{sgn}(\hat{x}_2) h, \tilde{\xi}_3 = B_2\Big), \tag{3}$$

where

$$\hat{x}_2 = \pm_2 \left(A_3 + \epsilon_1 f_3 \left(\theta_1 - \frac{1}{e_3} \ln r_1 \right) \right) r_1^{\delta_3},$$
$$\hat{x}_3 = \pm_3 \left(A_1 + \epsilon_1 f_1 \left(\theta_1 + \Phi_3 - \frac{1}{e_3} \ln r_1 - \frac{1}{e_1} \ln |\hat{x}_2| \right) \right) |\hat{x}_2|^{\delta_1},$$
$$\hat{\theta}_1 = \theta_1 + \Phi_1 + \Phi_2 + \Phi_3 - \frac{1}{e_3} \ln r_1 - \frac{1}{e_1} \ln |\hat{x}_2| - \frac{1}{e_2} \ln |\hat{x}_3| .$$

The trajectory visits $+E_2$ or $-E_2$ en route according to the sign of $\hat{x}_2$, and it returns to $+E_3$ or $-E_3$ according to the sign of $\hat{x}_3$. In this case, these signs are the same as the signs of x_2 and x_3. The map (3) can be simplified by assuming that A_3 and A_1 are order one and dropping the terms proportional to ϵ_1 in the expressions for $\hat{x}_2$ and $\hat{x}_3$. This results in an approximate map:

$$\begin{aligned} R(r_1, \theta_1, x_2 = \pm_2 h, \xi_3) = \Big(& \tilde{x}_1 = \epsilon_1 a_{\mathrm{r}} + A r_1^{\delta} \cos\left(\theta_1 + \Phi - Q \ln r_1\right), \\ & \tilde{y}_1 = \epsilon_1 a_{\mathrm{i}} + A r_1^{\delta} \sin\left(\theta_1 + \Phi - Q \ln r_1\right), \\ & \tilde{x}_2 = x_2, \tilde{\xi}_3 = B_2 \Big), \end{aligned} \tag{4}$$

where δ and Q were defined above, and A and Φ are constants as in equation (1).

Finally, when all symmetries are broken the return map is similar to the map (3) above, though with definitions of $\hat{x}_2$ and $\hat{x}_3$ that include terms proportional to ϵ_2 and ϵ_3:

$$\begin{aligned} \hat{x}_2 = & \pm_2 \left(A_3 + \epsilon_1 f_3 \left(\theta_1 - \frac{1}{e_3} \ln r_1 \right) \right) r_1^{\delta_3} \\ & + \epsilon_2 \left(1 + \epsilon_1 g_3 \left(\theta_1 - \frac{1}{e_3} \ln r_1 \right) \right), \\ \hat{x}_3 = & \pm_3 \left(A_1 + \epsilon_1 f_1 \left(\theta_1 + \Phi_3 - \frac{1}{e_3} \ln r_1 - \frac{1}{e_1} \ln |\hat{x}_2| \right) \right) |\hat{x}_2|^{\delta_1} \\ & + \epsilon_3 \left(1 + \epsilon_1 g_1 \left(\theta_1 + \Phi_3 - \frac{1}{e_3} \ln r_1 - \frac{1}{e_1} \ln |\hat{x}_2| \right) \right), \\ \hat{\theta}_1 = & \theta_1 + \Phi_1 + \Phi_2 + \Phi_3 - \frac{1}{e_3} \ln r_1 - \frac{1}{e_1} \ln |\hat{x}_2| - \frac{1}{e_2} \ln |\hat{x}_3| . \end{aligned} \tag{5}$$

The trajectory visits $+E_2$ or $-E_2$ en route according to the sign of $\hat{x}_2$, and it returns to $+E_3$ or $-E_3$ according to the sign of $\hat{x}_3$. It might seem that terms proportional to ϵ_1 in $\hat{x}_2$ and $\hat{x}_3$ could be dropped, as they were above. However, the terms $\pm_2 A_3 r_1^{\delta_3}$ and ϵ_2 could nearly cancel and likewise $\pm_3 A_1 |\hat{x}_2|^{\delta_1}$ and ϵ_3, so we do not drop the ϵ_1 terms. In fact, it turns out that retaining the ϵ_1 terms is essential for understanding the switching mechanisms.

It is possible to write down equivalent maps from $H_1^{\rm in} \to H_1^{\rm in}$ and $H_2^{\rm in} \to H_2^{\rm in}$. Note that the radial coordinates (as defined in the Appendix) play no role in the return maps, at the order to which we are working.

4 Analysis of return maps

Behaviour in the case without symmetry breaking is well understood and simple: whenever $\delta > 1$ and r is small, iteration of map (1) results in progressively smaller values of r and so there is an asymptotically stable heteroclinic cycle. The signs of x_2 and x_3 cannot change, owing to the presence of invariant subspaces, so each trajectory is confined to one quarter of the phase space. For the remainder of this section, we will assume $\delta > 1$.

4.1 *Global bifurcations*

Global bifurcations are a key ingredient for understanding the dynamics of the non-symmetric system. In this section, we describe the global bifurcations that are most important for our analysis.

4.1.1 ***Homoclinic bifurcation of P.*** The periodic orbit P has stable and unstable manifolds of dimension three and two, respectively, meaning that transverse intersections of the manifolds, when they occur, do so in a codimension-zero way, while tangencies between the manifolds will be of codimension one. Transverse homoclinic orbits can only occur when all symmetries are broken, as the following argument shows. If $\epsilon_2 = 0$, the subspace $x_2 = 0$ is invariant; since $\mathcal{W}^{\rm s}(P)$ lies in that subspace it cannot intersect $\mathcal{W}^{\rm u}(P)$. Similarly, if $\epsilon_3 = 0$, the subspace $x_3 = 0$ is invariant; since $\mathcal{W}^{\rm u}(P)$ lies in that subspace it cannot intersect $\mathcal{W}^{\rm s}(P)$. If $\epsilon_1 = 0$ then the rotation symmetry ensures that

any intersection of $\mathcal{W}^{\mathrm{u}}(P)$ and $\mathcal{W}^{\mathrm{s}}(P)$ will not be transverse.

In the case $\epsilon_1 = 0$, $\epsilon_2 \neq 0$, $\epsilon_3 \neq 0$, non-transversal homoclinic orbits of P occur when one branch of the stable manifold of P is coincident with one branch of the unstable manifold of P. This event can be located by calculating the image of $\mathcal{W}^{\mathrm{u}}(P)$ under $\Psi_{31} \circ \phi_3 \circ \Psi_{23} \circ \phi_2 \circ \Psi_{12}$ (see Appendix for definitions of the maps ϕ_i and Ψ_{ij}) and setting the x_2 component of the image to zero; we find that for small symmetry-breaking, non-transversal homoclinic bifurcations of P occur at

$$\epsilon_2 = -\pm_2 A_3 A_2^{\delta_3} |\epsilon_3|^{\delta_2 \delta_3}, \qquad \epsilon_1 = 0. \tag{6}$$

Homoclinic orbits can be formed by coincidence of either of the two branches of $\mathcal{W}^{\mathrm{u}}(P)$ with either of the two branches of $\mathcal{W}^{\mathrm{s}}(P)$, resulting in four possible homoclinic bifurcations corresponding to the four separate curves implicit in the expression above. These curves are shown as dashed lines in figure 3. The homoclinic orbit corresponding to the curve in the second quadrant of the (ϵ_2, ϵ_3) plane arises from the choice $\pm_2 = +$ and $\epsilon_3 > 0$, and passes close to $+E_2$ and $+E_3$; the three other bifurcation curves correspond to homoclinic orbits with the three other routes past the equilibria, in the obvious way.

As ϵ_1 changes from zero, each curve of non-transversal homoclinic bifurcations will generically split into two curves of homoclinic tangencies, with the region between the tangencies being parameter values for which there are transverse homoclinic orbits of P. Four curves of homoclinic tangencies and two regions of homoclinic tangles are shown schematically in figure 4.

Inspection of the expression for the x_2 component of the image of $\mathcal{W}^{\mathrm{u}}(P)$ under $\Psi_{31} \circ \phi_3 \circ \Psi_{23} \circ \phi_2 \circ \Psi_{12}$ gives more information about loci of the homoclinic bifurcations of P when $\epsilon_1 \neq 0$. This component can be written as:

$$\tilde{x}_2 = \pm_2 R_1^{\delta_3} \left(A_3 + \epsilon_1 f_3(\Theta_1) \right) + \epsilon_2 \left(1 + \epsilon_1 g_3(\Theta_1) \right), \tag{7}$$

where R_1 and Θ_1 are complicated functions of the coefficients and parameters. In this expression, $A_3 + \epsilon_1 f_3(\Theta_1)$ must remain positive, as explained in the Appendix, and R_1 is positive. Expressions for the positions of the homoclinic tangencies in parameter space can be calculated by setting $\tilde{x}_2 = 0$; these expressions are not included here due to their extreme ugliness. Nonetheless, we note that for ϵ_1 small, when $\pm_2 = +$, there are only solutions with $\epsilon_2 < 0$;

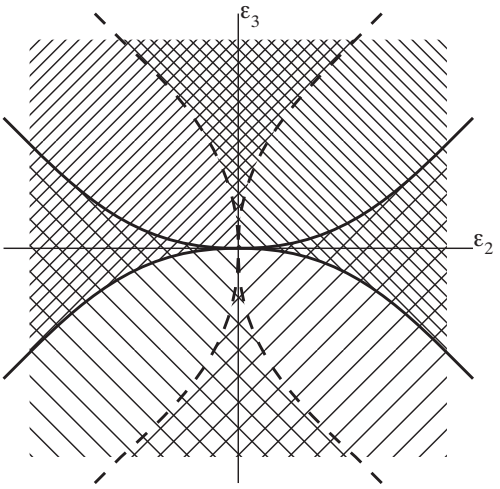

Figure 3. Schematic bifurcation set for the case $\epsilon_1 = 0$, ϵ_2 and ϵ_3 small. Regions of asymptotically stable quasiperiodic solutions are bounded by codimension-one curves of global bifurcations, i.e., non-transverse homoclinic bifurcations of P (dashed curves) and heteroclinic bifurcations of the cycles $\pm E_2 \to \pm E_3 \to \pm E_2$ (solid curves). The shapes of the global bifurcation curves correspond to the choice $\delta_1 > 1$, $\delta_2 > 1$ and $\delta_3 > 1$, but similar figures could be drawn for the other cases. As explained in Section 4.2, the various shading styles indicate the regions in which four different quasiperiodic solutions occur. Close to the ϵ_2 and ϵ_3 axes, two different quasiperiodic solutions coexist.

this is consistent with figures 3 and 4, in which each bifurcation curve is confined to a single quadrant. However, if ϵ_1 is large enough that $1 + \epsilon_1 g_3(\Theta_1)$ can change sign as Θ_1 varies, the loci of the homoclinic bifurcations of P can change quadrants. Of course, this effect is outside the range of validity of the return maps we have constructed, but the principle is worth bearing in mind as it appears to influence the dynamics observed in the numerical example discussed in Section 5.

4.1.2 ***Heteroclinic bifurcation*** $\boldsymbol{\pm E_2 \to \pm E_3 \to \pm E_2}$**.** In the case that all symmetries are broken, consideration of the dimensions of the stable and unstable manifolds of the equilibrium points shows that the heteroclinic cycle $+E_2 \to +E_3 \to +E_2$ will occur in a codimension-two manner. However, if $\epsilon_1 = 0$, the connection $+E_2 \to +E_3$ is robust and the intersection of $\mathcal{W}^{\mathrm{u}}(+E_3)$ and $\mathcal{W}^{\mathrm{s}}(+E_2)$ is a codimension-one phenomenon, meaning that the heteroclinic cycle as a whole occurs with codimension one. This latter case is of interest since, as we will see, the heteroclinic bifurcation unfolds when $\epsilon_1 \neq 0$

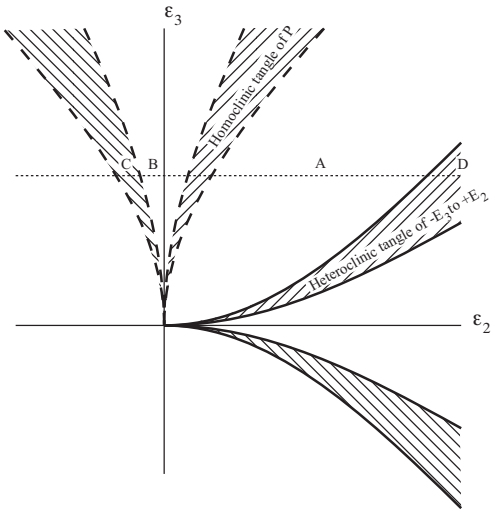

Figure 4. Schematic diagram showing part of the bifurcation set for the case ϵ_1 fixed and non-zero but small (compare with figure 3). Dashed curves correspond to homoclinic tangencies of P, solid curves in the first (resp. fourth) quadrant correspond to heteroclinic tangencies between $\mathcal{W}^{\mathrm{u}}(-E_3)$ (resp. $\mathcal{W}^{\mathrm{u}}(+E_3)$) and $\mathcal{W}^{\mathrm{s}}(+E_2)$, and the shading shows regions in which the corresponding homoclinic or heteroclinic tangles exist. The dotted horizontal line indicates a path through parameter space discussed in Section 4.4; the labels A – D indicate schematically parameter values used in section 5.

into homoclinic bifurcations of $+E_2$ and $+E_3$ and heteroclinic tangencies between $\mathcal{W}^{\mathrm{u}}(+E_3)$ and $\mathcal{W}^{\mathrm{s}}(+E_2)$ similar to the way each non-transverse homoclinic bifurcation of P splits into two homoclinic tangencies when ϵ_1 is varied from zero (see above). An analogous argument works for heteroclinic cycles involving $-E_2$ and/or $-E_3$.

Calculations with the local and global maps yields an expression for the parameter values at which these heteroclinic bifurcations occur:

$$\epsilon_3 = -\pm_3 A_1 |\epsilon_2|^{\delta_1}, \qquad \epsilon_1 = 0.$$

See figure 3. This expression is valid for all four cycles $\pm E_2 \to \pm E_3 \to \pm E_2$ so long as $\pm_3$ and the sign of ϵ_2 are chosen appropriately.

4.1.3 ***Homoclinic bifurcations of $\pm E_2$ and $\pm E_3$.*** The dimensions of the stable and unstable manifolds of $\pm E_2$ and $\pm E_3$ are such that if homoclinic bifurcations of these equilibria occur, they are of codimension one.

An argument similar to that used in subsection 4.1.1 shows that we require

$\epsilon_1 \neq 0$ and $\epsilon_3 \neq 0$ if a homoclinic bifurcation of $\pm E_2$ is to occur, although ϵ_2 could be zero. Similarly, existence of a homoclinic bifurcation of $\pm E_3$ requires $\epsilon_1 \neq 0$ and $\epsilon_2 \neq 0$, although ϵ_3 could be zero. The homoclinic bifurcations of $\pm E_2$ (resp. $\pm E_3$) will be of Shil'nikov type if $\delta_2 < 1$ (resp. $\delta_3 < 1$) and if $c_2 < 2$ (resp. $c_3 < 2$) [34].

We can in principle calculate parameter values at which these homoclinic bifurcations occur, but the expressions are too nasty to be useful. Instead, we note that there can be two homoclinic bifurcations of $+E_2$, one for each branch of the unstable manifold of $+E_2$, and a further two homoclinic bifurcations of $-E_2$. Similarly, there can be two homoclinic bifurcations of $+E_3$ and two homoclinic bifurcations of $-E_3$. These eight homoclinic bifurcations will in general occur at different parameter values, but in the limit $\epsilon_1 \to 0$, will converge pairwise on the loci of the four heteroclinic bifurcations involving $\pm E_2$ and $\pm E_3$ discussed in the previous subsection. For instance, as $\epsilon_1 \to 0$, a homoclinic orbit of $+E_2$ passing near $-E_3$ and a homoclinic orbit of $-E_3$ passing near $+E_2$ will converge in phase space on the heteroclinic cycle $+E_2 \to -E_3 \to +E_2$, and the parameter values at which the homoclinic bifurcations occur will converge in parameter space on the locus of the heteroclinic bifurcation. For clarity, these bifurcation curves are not shown in figure 4.

The dynamics associated with these bifurcations will be discussed further below.

4.2 *Breaking the two reflection symmetries*

Here we show that, for $\epsilon_1 = 0$ and for sufficiently small ϵ_2 and ϵ_3, map (2) generically has at least one asymptotically stable closed invariant curve and the corresponding flow has quasiperiodic solutions. This is not a surprising result, since the coordinate θ_1 decouples from the other coordinates when $\epsilon_1 = 0$, in which case our system can be reduced to a three-dimensional system with a SSHC between equilibria; earlier work on a system related to our reduced system showed that breaking the reflection symmetries can give rise to asymptotically stable periodic solutions [19]. Our main aim in this section is to locate the regions in parameter space in which the quasiperiodic solutions exist, for comparison with the location of some of the global bifurcations described in section 4.1.

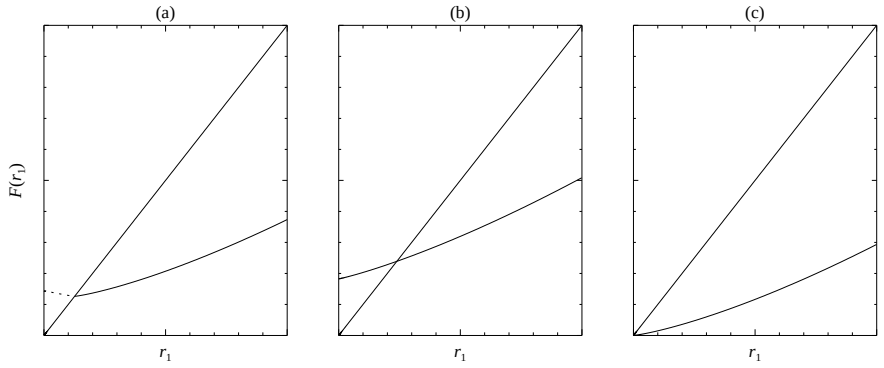

Figure 5. Schematic graphs of $F(r_1)$ (equation (8)) for the choice $\pm_2 = \pm_3 = 1$ when $\delta_1 > 1$, $\delta_2 > 1$, $\delta_3 > 1$, and $A_1 = A_2 = A_3 = 1$. The solid (resp. dotted) curve indicates values of r_1 for which the next values of $\pm_2$ and $\pm_3$ are (resp. are not) both positive; we seek values of r_1 for which the solid curve intersects the diagonal. For small positive ϵ_2 and ϵ_3, a stable fixed point exists (see panel (b)). This fixed point ceases to exist in the second quadrant when $\epsilon_2 = -A_3 A_2^{\delta_2} \epsilon_3^{\delta_2 \delta_3}$, when there is a non-transversal homoclinic bifurcation of P (limiting case shown in panel (a)). The fixed point is destroyed in the fourth quadrant when $\epsilon_3 = -A_1 \epsilon_2^{\delta_1}$, when there is a non-transversal heteroclinic connection from $+E_3$ to $+E_2$ (limiting case shown in panel (c)).

The r_1 component of map (2) is independent of the other variables, and so we first seek values of r_1 for which $F(r_1) = r_1$, where

$$F(r_1) = A_2 \Big| \epsilon_3 \pm_3 A_1 \big| \epsilon_2 \pm_2 A_3 r_1^{\delta_3} \big|^{\delta_1} \Big|^{\delta_2}. \tag{8}$$

For each choice of ϵ_2 and ϵ_3, there are two possible signs of each of $\pm_2$ and $\pm_3$, but the case $(\pm_2 = +, \epsilon_2 > 0)$ is equivalent to $(\pm_2 = -, \epsilon_2 < 0)$, and the case $(\pm_3 = +, \epsilon_3 > 0)$ is equivalent to $(\pm_3 = -, \epsilon_3 < 0)$. Without loss of generality, we focus on the case $\pm_2 = +$, $\pm_3 = +$, and seek values of ϵ_2 and ϵ_3 for which there exist fixed points of map (8). Fixed points of this type have positive values within the absolute value signs in (8), since the signs of $\epsilon_2 + A_3 r_1^{\delta_3}$ and $\epsilon_3 + A_1 |\epsilon_2 + A_3 r_1^{\delta_3}|^{\delta_1}$ determine the next values of $\pm_2$ and $\pm_3$.

For sufficiently small, positive ϵ_2 and ϵ_3, $F(0) = A_2(\epsilon_3 + A_1 \epsilon_2^{\delta_1})^{\delta_2} > 0$. For r_1 larger than ϵ_2 and ϵ_3 but still smaller than one, we have $F(r_1) \sim r_1^{\delta}$, which is less than r_1 since $\delta > 1$. Thus, by continuity, the map has a fixed point (see figure 5(b)). Since $F(r_1)$ is monotonically increasing, the slope of F at the fixed point is less than one, so a stable fixed point exists for $\epsilon_2 > 0$, $\epsilon_3 > 0$.

This fixed point (i.e., a fixed point with $\pm_2 = \pm_3 = +$) also exists in parts of the second and fourth quadrants of the (ϵ_2, ϵ_3) parameter plane. To determine

the region of existence in the fourth quadrant, we fix ϵ_2 at some small positive value and decrease ϵ_3. This shifts the graph of $F(r_1)$ down, from which it is found that a stable fixed point exists until $F(0) = 0$, i.e., until $\epsilon_3 = -A_1\epsilon_2^{\delta_1}$ (figure 5(c)). Thus the fixed point ceases to exist in the fourth quadrant at the locus of the heteroclinic bifurcation from $+E_3$ to $+E_2$ (c.f. section 4.1.2).

To determine where the fixed point exists in the second quadrant, we fix ϵ_3 at some small positive value and decrease ϵ_2. This decreases $F(0)$ and also changes the shape of the graph of $F(r_1)$; the graph remains monotonic increasing in r_1 while ϵ_2 is positive, but develops a turning point once ϵ_2 becomes negative, with $F(r_1)$ decreasing for r_1 near zero. The decreasing section is indicated by a dotted curve in figure 5(a), and corresponds to future values of $\pm_2$ and $\pm_3$ not both being positive. For small enough negative ϵ_2 the dotted section of the graph lies to the left of fixed point, but when $\epsilon_2 = -A_3A_2^{\delta_2}\epsilon_3^{\delta_2\delta_3}$, the dotted curve reaches to the diagonal and the fixed point ceases to exist (figure 5(a)). Thus the fixed point ceases to exist in the second quadrant on the locus of the homoclinic bifurcation of P (c.f. section 4.1.1).

The region of existence of this stable fixed point is indicated by the left-leaning close hatching in figure 3. Calculations with the other combinations of signs of $\pm_2$ and $\pm_3$ are analogous, and yield different regions of existence for the corresponding fixed points. Fixed points may coexist as shown in figure 3.

Since for fixed r_1 the θ_1 component of map (2) is a rigid rotation, a fixed point of equation (8) generically corresponds to a closed invariant curve in (2) and to a quasiperiodic solution in the full flow. The angle θ_1 decouples from the rest of the dynamics, and so the full flow will have an invariant torus foliated by periodic orbits for a dense set of parameter values. Stability of these solutions follows from the stability of the fixed point of (8).

The calculations above were for the case $\delta_1 > 1$, $\delta_2 > 1$, $\delta_3 > 1$. Similar calculations done when one or more of the δ_i is smaller than one lead to similar regions of existence of quasiperiodic solutions, except that there are additional saddle-node bifurcations of the tori close to the relevant global bifurcations; these saddle-node bifurcations arise since the global bifurcations destroy solutions of different stabilities depending on the sign of $\delta_i - 1$.

The special case that precisely one of ϵ_2 and ϵ_3 is zero (i.e., only one reflection symmetry is broken) is covered by the analysis above; there will be two fixed points of the map with corresponding (foliated) tori in the flow.

In summary, when the two reflection symmetries are broken but the rotation symmetry is preserved, the flow generically has asymptotically stable quasiperiodic solutions that do not exhibit switching. Different quasiperiodic solutions coexist in regions bounded by global bifurcations that will play an important role in generating complex dynamics when $\epsilon_1 \neq 0$.

4.3 *Breaking the rotation symmetry*

In this subsection we show that for sufficiently small values of ϵ_1, with $\epsilon_2 = \epsilon_3 = 0$, the map (4) has a stable fixed point.

By rescaling r_1 and ϵ_1 by order one amounts and moving the origin of the θ_1 coordinate, we can without loss of generality set $A = 1$, $a_\mathrm{r} = 1$ and $a_\mathrm{i} = 0$ in (4). Ignoring for now the x_2 and ξ_3 components of the map and working with polar coordinates (ρ, ϕ) centred at $(x_1, y_1) = (\epsilon_1, 0)$ (so that $x_1 = \epsilon_1 + \rho\cos\phi$ and $y_1 = \rho\sin\phi$), map (4) reduces to

$$\begin{cases} \tilde{x}_1 = \epsilon_1 + \tilde{\rho}\cos\tilde{\phi} \\ \tilde{y}_1 = \qquad \tilde{\rho}\sin\tilde{\phi} \end{cases} \qquad \text{where} \qquad \begin{cases} \tilde{\rho} = r_1^\delta \\ \tilde{\phi} = \theta_1 + \Phi - Q\ln r_1. \end{cases} \tag{9}$$

The constant Φ may take a different value here than in equations (4). Fixed points of (9) satisfy $r_1 = \sqrt{\tilde{x}_1^2 + \tilde{y}_1^2}$ and $\theta_1 = \arctan(\tilde{y}_1/\tilde{x}_1)$. To find solutions of the first of these equations, note that circles of radius r about $(x_1, y_1) = (0, 0)$ map under (9) to circles of radius r^δ about $(\epsilon_1, 0)$. Since $\delta > 1$ and for small r, these circles will intersect if $r \geq \epsilon_1 - r^\delta$ and $r \leq \epsilon_1 + r^\delta$; the intersection points are candidate fixed points of the map. For each small fixed value of ϵ_1, there will be some non-zero interval $a \leq r \leq b$ on which the inequalities are both satisfied. See figure 6(a–c).

The second equation, $\theta_1 = \arctan(\tilde{y}_1/\tilde{x}_1)$, is satisfied for at least one value of r in $[a, b]$, as the following argument shows. When $r = a$, the circles $(r_1, \theta_1) = (r, \theta_1)$ and $(\rho, \phi) = (r^\delta, \phi)$ intersect at a single point, $(r_1, \theta_1) = (a, 0)$, alternatively $(\rho, \phi) = (a^\delta, \pi)$. As r is increased beyond a, the intersection point splits into two (with corresponding ϕ values just below π and just above $-\pi$). The intersection points come together again at $(r_1, \theta_1) = (b, 0)$ or $(\rho, \phi) = (b^\delta, 0)$, in the manner shown in figure 7(a). The corresponding value of $\tilde{\phi}$ for each intersection point can be calculated from (9) (see figure 7(b))

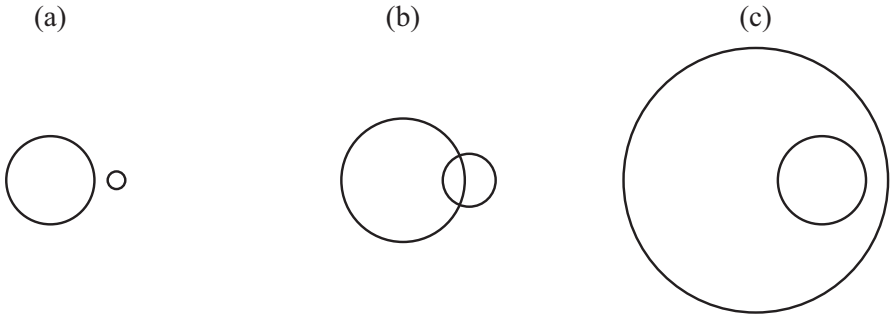

Figure 6. Finding fixed points of equations (9). Panels (a–c) show schematically the relative positions of the circle of radius r around $(x_1, y_1) = (0, 0)$ (large circle in each panel) and its image under map (9) for various sizes of r: (a) $r < \epsilon_1 - r^\delta$, no intersection; (b) $r \geq \epsilon_1 - r^\delta$ and $r \leq \epsilon_1 + r^\delta$, one or two intersections; (c) $r > \epsilon_1 + r^\delta$, no intersections.

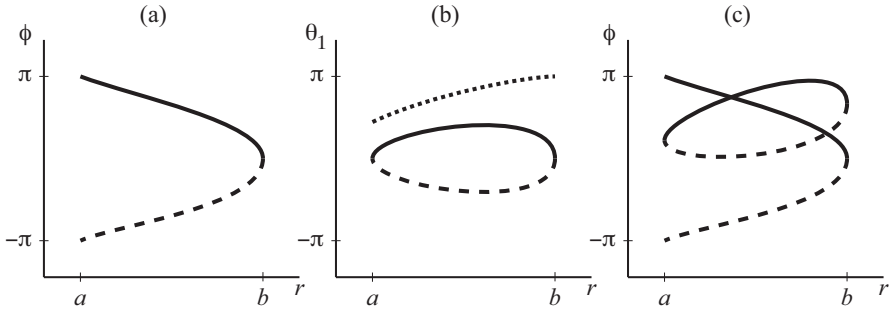

Figure 7. (a) Schematic ϕ values for intersections of the two circles $(r_1, \theta_1) = (r, \theta_1)$ and $(\rho, \phi) = (r^\delta, \phi)$, in the situation shown in figure 6(b), plotted as a function of r; (b) Schematic showing θ_1 (solid and dashed curves) and $-Q \ln r_1$ (dotted curve) for points of intersection of the two circles, plotted as a function of r at the intersection points; (c) ϕ and $\tilde{\phi}$ values at points of intersection of the two circles. Solid curves correspond to the upper intersection points and their images, dashed curves correspond to the lower intersection points and their images.

from which it is seen that the two branches of $\tilde{\phi}$, arising from the upper and lower intersections of the two circles, start and end at the same point as each other, as shown in figure 7(c). At least one of the two branches of the graph of $\tilde{\phi}$ vs r therefore intersects the graph of ϕ vs r for that same branch for at least one r in $[a, b]$. Thus, there is at least one fixed point of the map (9).

It is straightforward to show that the determinant of the Jacobian of map (9) is $\delta r^{2(\delta-1)}$ and that the absolute value of the trace of the Jacobian is bounded above by $\sqrt{(\delta+1)^2 + Q^2}\, r^{\delta-1}$. For each choice of ϵ_1, the value of r at the corresponding fixed point lies in $[a, b]$, where a and b depend on ϵ_1 with $a > 0$ and a and b tending to zero as $\epsilon_1 \to 0$. Thus, for sufficiently small ϵ_1, the

determinant and trace of the linearised map are small enough to ensure that the relevant fixed point is stable. It follows that the corresponding fixed point of equations (4) is also stable, since orbits of that map collapse onto a constant value of the third (radial) coordinate after one iteration of the map.

In summary, for sufficiently small ϵ_1 when $\epsilon_2 = \epsilon_3 = 0$, the heteroclinic cycle that occurred in the fully symmetric case is replaced by a stable periodic orbit. Using the reflection symmetries κ_2 and κ_3, we find four stable periodic orbits co-exist, one in each quarter of the phase space.

4.4 *Breaking all symmetries*

Direct analysis of the return map valid for the case that all symmetries are broken is not feasible because of the extremely complicated form of that map. Instead, in this section we use our knowledge of the dynamics in the case $\epsilon_1 = 0$ and arguments about generic unfoldings of this special case to deduce what types of dynamics will be seen in the fully asymmetric case for ϵ_1 near zero, and to (approximately) locate each type of behaviour in parameter space. This procedure allows us to make specific predictions about the mechanisms underlying the complicated dynamics observed in numerical examples, such as the example described in section 5. We are especially interested in finding mechanisms that cause repeated, non-periodic switching in our system.

The dynamics associated with the case $\epsilon_1 = 0$ is summarised in figure 3, which shows eight curves of global bifurcations bounding regions in which there are asymptotically stable quasiperiodic solutions. In this case the rotation symmetry prevents coupling of the two frequencies associated with each quasiperiodic solution and the dynamics is simple. Once ϵ_1 moves away from zero, we will generically see locking of the frequencies. For instance, if we were to fix ϵ_1 sufficiently small but non-zero and pick ϵ_2 and ϵ_3 positive and with values midway between the two pairs of global bifurcation curves in the first quadrant of figure 4, then along a one-dimensional path through the parameter space such as the dotted line in figure 4 there will be intervals of quasiperiodicity interspersed with intervals of locked, periodic behaviour. Associated with the frequency locking there may be complicated dynamics such as period-doubling cascades and chaotic dynamics. However, this behaviour will mostly be confined to regions of phase space near the original quasiperiodic solutions,

and is not the main mechanism for switching in our system.

As shown in section 4.1.1 and in figure 4, each curve of non-transverse homoclinic bifurcations of P seen in figure 3 turns into a wedge in parameter space of transverse homoclinic orbits of P when ϵ_1 changes from zero. There will be horseshoes and chaotic dynamics associated with the transverse homoclinic orbits, although the chaos may not be attracting. In numerical examples we might expect to see a mixture of stable periodic orbits and stable chaotic dynamics, in overlapping regions of parameter space.

An interesting consequence of the occurrence of homoclinic tangles is that it provides a mechanism for switching of orbits with respect to the x_2 variable. For instance, for sufficiently small ϵ_1, and with $\epsilon_2 > 0$, $\epsilon_3 > 0$ and both small, solutions that make excursions near $+E_2$ can get trapped. The trapping region is bounded in part by one branch of $\mathcal{W}^{\mathrm{s}}(P)$ and trapped solutions make excursions past $+E_2$ but cannot cross $\mathcal{W}^{\mathrm{s}}(P)$ so cannot get close to $-E_2$. If ϵ_2 is decreased, say by moving along the dotted path shown in Figure 4 into the homoclinic wedge in the second quadrant, the trapping region develops a leak when a homoclinic tangency forms between that branch of $\mathcal{W}^{\mathrm{s}}(P)$ and a branch of $\mathcal{W}^{\mathrm{u}}(P)$; solutions are then able to cross $\mathcal{W}^{\mathrm{s}}(P)$, and may visit a neighbourhood of $-E_2$. We call this 'switching in x_2'. Switching of this type (from positive to negative x_2) can occur for parameter values to the left of the right boundary of the homoclinic wedge in the second quadrant. A numerical example of this leaking process is given below in figure 9.

Once a switching solution arrives in the region with $x_2 < 0$, it may then get captured by an attractor lying solely in the negative x_2 region of phase space, in which case no more switching will be observed. Alternatively, if there is a mechanism for orbits to leak back to the original region of phase space then there could be sustained switching in x_2. This latter case cannot occur for arbitrarily small ϵ_1 as the following argument shows. For the case $\epsilon_1 = 0$, results from section 4.2 show that orbits which make repeated excursions near $-E_2$ and $+E_3$ occur in the second quadrant of figure 4 and in the first quadrant as far as the locus of homoclinic bifurcations of P. (This homoclinic bifurcation involves a different branch of $\mathcal{W}^{\mathrm{u}}(P)$ than the homoclinic bifurcation occurring for $\epsilon_2 < 0$ discussed in the last paragraph.) For small ϵ_1, there will be a wedge of homoclinic tangencies of the relevant branches of $\mathcal{W}^{\mathrm{u}}(P)$ and $\mathcal{W}^{\mathrm{s}}(P)$, with the wedge lying entirely within the region $\epsilon_2 > 0$, $\epsilon_3 > 0$; orbits that make

a number of excursions past $-E_2$ before switching and passing close to $+E_2$ can only occur for values of ϵ_2 and ϵ_3 lying to the right of the left boundary of the wedge. Thus, for sufficiently small ϵ_1, there is no overlap between the region of parameter space where there is switching from positive to negative x_2 and the region where there is switching from negative to positive x_2, with the consequence that there can be no sustained switching in x_2.

However, as argued in section 4.1.1, for large enough ϵ_1 the curves of homoclinic tangency may change quadrants in the (ϵ_2, ϵ_3) parameter plane, and then the switching regions can overlap, making sustained switching in x_2 possible. As pointed out in section 4.1.1, our return map construction is not valid for 'large' ϵ_1, so we have not proved the existence of sustained switching, just shown how it might feasibly occur. It is not possible to determine a priori how big ϵ_1 would have to be to get sustained switching, but we have shown that there is a threshold in ϵ_1 below which sustained switching in x_2 is not possible. The value of this threshold does not go to zero as ϵ_2 and ϵ_3 go to zero, as it comes from the requirement that $1 + \epsilon_1 g_3(\Theta_1)$ changes sign (as a function of Θ_1) in equation (7). Another way of understanding this is to note that in (7), if $\pm_2 = +$ and $\epsilon_2 > 0$, then the only way of having $\tilde{x}_2$ negative is to have $1 + \epsilon_1 g_3(\Theta_1) < 0$ for some value of Θ_1. This is a necessary but not sufficient condition, as the attractor may not explore the required range of Θ_1.

The four curves of heteroclinic bifurcations of the cycles $\pm E_2 \to \pm E_3 \to \pm E_2$ shown in figure 3 also split when ϵ_1 becomes non-zero, being replaced by eight curves of homoclinic bifurcations and eight curves of heteroclinic tangencies between $\mathcal{W}^{\mathrm{u}}(\pm E_3)$ and $\mathcal{W}^{\mathrm{s}}(\pm E_2)$, as described in section 4.1.2. If they are of Shil'nikov type, the homoclinic bifurcations can complicate the dynamics by inducing chaotic dynamics. The heteroclinic bifurcations are associated with switching in the x_3 coordinate similarly to the way switching in x_2 is associated with homoclinic bifurcations of P, described above. More precisely, the eight curves of heteroclinic tangencies between $\mathcal{W}^{\mathrm{u}}(\pm E_3)$ and $\mathcal{W}^{\mathrm{s}}(\pm E_2)$ come in pairs, with each pair bounding a wedge in parameter space. At parameter values within each wedge there is a heteroclinic tangle of one pair of manifold branches. For instance, for sufficiently small ϵ_1 there will be a heteroclinic wedge involving one branch of $\mathcal{W}^{\mathrm{u}}(+E_3)$ and one branch of $\mathcal{W}^{\mathrm{s}}(+E_2)$ occurring in the fourth quadrant in the (ϵ_2, ϵ_3) plane. Above this wedge, $\mathcal{W}^{\mathrm{s}}(+E_2)$ bounds in part a trapping region; orbits in the trapping region make excur-

sions past $+E_3$ but cannot cross $\mathcal{W}^{\mathrm{s}}(+E_2)$ to get close to $-E_3$. The trapping region develops a leak when a heteroclinic tangency forms between the appropriate branches of $\mathcal{W}^{\mathrm{u}}(+E_3)$ and $\mathcal{W}^{\mathrm{s}}(+E_2)$ thus allowing solutions to cross $\mathcal{W}^{\mathrm{s}}(+E_2)$. We call this 'switching in x_3'. An argument analogous to that used for switching in x_2 can be used here to show that there is a (generically different) threshold in ϵ_1 below which there can be no persistent switching in x_3. This threshold does not go to zero when ϵ_2 and ϵ_3 go to zero.

The mechanisms inducing switching in x_2 and in x_3 are distinct, but orbits that switch persistently in both x_2 and x_3 are possible for ϵ_1 above the thresholds for both mechanisms. Switching in each variable requires the rotation and appropriate reflection symmetry to be broken. It is possible to have persistent switching in x_2 with $\epsilon_3 = 0$, or switching in x_3 with $\epsilon_2 = 0$, though we will not explore this possibility in detail. The example in section 5 shows that persistent switching is easily observed in numerical examples.

Both of the global bifurcations we have identified as inducing switching, i.e., homoclinic tangencies of $\mathcal{W}^{\mathrm{u}}(P)$ and $\mathcal{W}^{\mathrm{s}}(P)$ and heteroclinic tangencies of $\mathcal{W}^{\mathrm{u}}(\pm E_3)$ and $\mathcal{W}^{\mathrm{s}}(\pm E_2)$, will produce horseshoes in the dynamics. In the case of homoclinic tangencies, this is a standard result and in the case of the heteroclinic tangencies, reinjection into the neighbourhood of the heteroclinic tangle is provided by proximity in phase and parameter space to the heteroclinic cycle $\pm E_2 \to \pm E_3 \to \pm E_2$. In either case, we expect the onset of switching to be commonly associated with nearby chaotic dynamics; chaotic orbits before the onset of switching, chaotic transients for switching orbits and orbits that switch chaotically might all be seen. However, other types of switching are also possible, such as periodic switching where the attractor is a periodic orbit that crosses the (non-invariant) hyperplanes $x_2 = 0$ and $x_3 = 0$ or periodic switching where the attractor is a 'noisy periodic orbit' such as results from a cascade of period doubling. In the latter case the itinerary of visits to $\pm E_2$ or $\pm E_3$ will be periodic even though the actual orbits are not.

5 Example

We consider the following system of equations to illustrate the dynamics of interest in this paper:

$$\dot{z}_1 = (1+\mathrm{i})z_1 - |z_1|^2 z_1 - (c_2+1)x_2^2 z_1 + (e_3-1)x_3^2 z_1 + \epsilon_1 d_{11} + \epsilon_1 d_{12} x_1 \,, \tag{10}$$

$$\dot{x}_2 = x_2 - x_2^3 - (c_3+1)x_3^2 x_2 + (e_1-1)|z_1|^2 x_2 + \epsilon_2 d_{21} + \epsilon_1 d_{22} x_1 x_2 + \epsilon_1\epsilon_2 d_{23} x_1 \,, \tag{11}$$

$$\dot{x}_3 = x_3 - x_3^3 - (c_1+1)|z_1|^2 x_3 + (e_2-1)x_2^2 x_3 + \epsilon_3 d_{31} + \epsilon_1 d_{32} x_1 x_3 + \epsilon_1\epsilon_3 d_{33} x_1 \,, \tag{12}$$

These equations were derived by starting with the structurally stable heteroclinic cycle considered in [2], turning a pair of equilibria of that cycle into a periodic orbit by adding a trivial phase variable, and adding the simplest possible terms that break the symmetries in generic ways. The parameters ϵ_1, ϵ_2 and ϵ_3 in equations (10–12) play the same role as in the maps derived earlier in this paper.

The model used in [20] is similar, but differs in two respects. First, the symmetry-breaking terms in [20] were fifth-order in the x and z variables, rather than constant, linear and quadratic here. Second, the model in [20] respects the symmetry $(z_1, x_2, x_3) \to (-z_1, -x_2, -x_3)$, as appropriate for a model of a dynamo instability: the invariant subspace $z_1 = x_2 = x_3 = 0$ corresponds to the absence of any magnetic field. We do not expect the first difference between models to alter the qualitative behaviour, but the enforced symmetry may have a significant effect, as discussed briefly in the next section.

The coefficients in the equations were chosen to be: $c_1 = 1.2$, $e_1 = 1.0$, $c_2 = 1.1$, $e_2 = 1.0$, $c_3 = 1.1$, $e_3 = 1.0$ for the contracting and expanding eigenvalues, and $d_{11} = d_{12} = 10^{-4}$, $d_{21} = 10^{-1}$, $d_{22} = 10^{-1}$, $d_{23} = 10^{3}$, $d_{31} = 10^{-3}$, $d_{32} = 10^{-4}$, $d_{33} = 1$ for the symmetry-breaking coefficients. The eigenvalues were chosen to be of order one, with contraction dominating expansion at each point ($\delta_1 = 1.2$, $\delta_2 = 1.1$, $\delta_3 = 1.1$, and an overall $\delta = 1.452$). The symmetry breaking coefficients are notionally small, but those coefficients (d_{23} and d_{33}) that are multiplied by two ϵ's were chosen to be larger to compensate for this. The exact numbers are not important, though they will affect the details of

what is observed. However, choosing d_{23} and d_{33} to be reasonably large means that the switching dynamics is easier to obtain for small values of ϵ_1: in order to get persistent switching, the $\epsilon_1\epsilon_2 d_{23}x_1$ and $\epsilon_1\epsilon_3 d_{33}x_1$ terms in (10–12) need to be reasonably important.

We integrated the equations numerically using the Bulirsch–Stoer adaptive integrator [35], with a tolerance for the relative error set to 10^{-12} for each step. Poincaré sections were computed using algorithms from [36].

By varying ϵ_1, ϵ_2 and ϵ_3, we are able to find examples of the important symmetry-breaking effects discussed in the previous sections of this paper. The cases with full or partial symmetry preserved give straightforward results, which we describe only briefly; more details are provided of the case of fully broken symmetry.

If all symmetries are preserved (all $\epsilon_i = 0$) then each solution starting off the invariant subspaces is attracted to one of four symmetry-related structurally stable heteroclinic cycles. If $\epsilon_1 \neq 0$, $\epsilon_2 = \epsilon_3 = 0$ (rotation symmetry broken, reflections preserved), numerics confirm the predictions of section 4.3, and a single attracting periodic orbit is found in each quarter of the phase space. If rotation symmetry is preserved as well as one reflection, and the other reflection is broken, then solutions are attracted to a foliated torus, as discussed in section 4.2. In the case that both reflections are broken but the rotation symmetry is preserved, numerics confirm the predictions of section 4.2; we find that there exist attracting quasiperiodic solutions in regions bounded by curves of global bifurcations, as shown schematically in figure 3. Analysis of the maps derived earlier allows us to predict scaling of the loci of various global bifurcations in the limit of small symmetry breaking. For instance, equation (6) tells us that for $\epsilon_1 = 0$ and $\epsilon_3 \to 0$, homoclinic bifurcations of P associated with equations (10–12) occur for $\epsilon_2 = \text{constant} \times |\epsilon_3|^{\delta_2\delta_3}$ but the value of the constant is not determined by the map analysis. Numerical simulations of equations (10–12) confirm the scalings for the various global bifurcations.

To illustrate the phenomena associated with breaking all symmetries, it is helpful to consider the changes in dynamics seen along a one-dimensional path such as that shown as the dotted line in figure 4. We first chose a value of ϵ_1 below the thresholds for persistent switching in x_2 and x_3. For instance, fixing $\epsilon_1 = 10^{-4}$ and $\epsilon_3 = 0.001$ and allowing ϵ_2 to vary, we see the following types of dynamics.

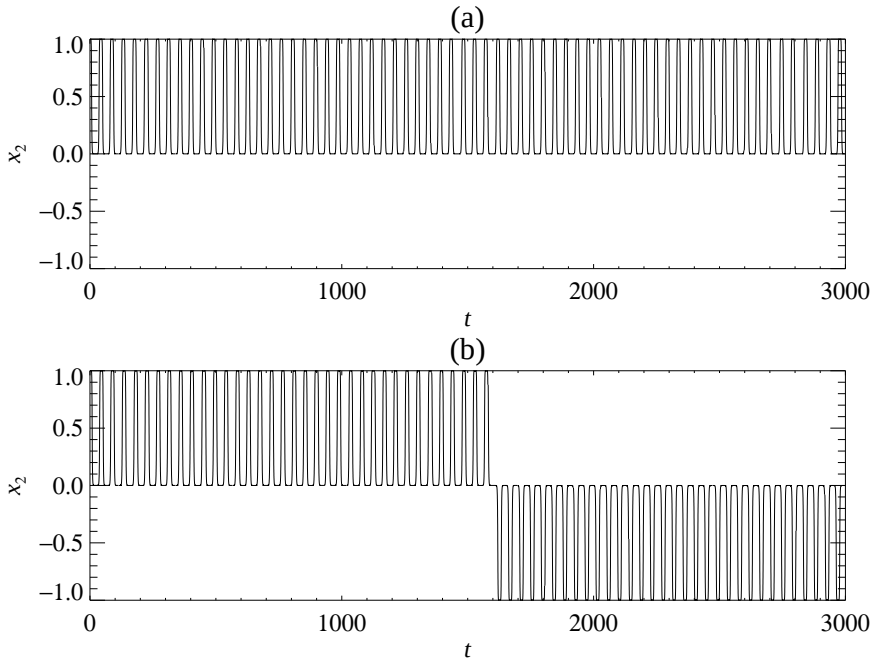

Figure 8. Onset of switching in x_2 for equations (10–12), associated with crossing into the wedge of homoclinic bifurcations of P in the second quadrant of (ϵ_2, ϵ_3)-space. Parameters $\epsilon_1 = 10^{-4}$, $\epsilon_3 = 0.001$ are fixed and ϵ_2 is decreased: (a) $\epsilon_2 = -5.67 \times 10^{-7}$ gives a chaotic attractor confined to the region $x_2 > 0$; (b) $\epsilon_2 = -5.68 \times 10^{-7}$ gives a chaotic transient with $x_2 > 0$, then the sign of x_2 changes and the orbit is attracted to a quasiperiodic solution with $x_2 < 0$. Other coefficients as described in text. The chaotic nature of the orbit in (a) and the transient in (b) is not apparent on the timescale used to plot the time series.

Picking $\epsilon_2 = 3 \times 10^{-5}$ yields a point (labelled A) lying to the right of the homoclinic wedge and to left of the heteroclinic wedge in the first quadrant of figure 4. For these ϵ_2 and ϵ_3 values but for $\epsilon_1 = 0$, there exists an attracting quasiperiodic solution with x_2 and x_3 both positive. With $\epsilon_1 = 10^{-4}$ the same type of quasiperiodic solution exists. As ϵ_2 is decreased while ϵ_1 is fixed at 10^{-4} we find, as expected, intervals of ϵ_2 in which there are quasiperiodic attractors interspersed with intervals on which there is locking of the two frequencies associated with the quasiperiodic solution (periodic orbits). In some intervals, period doubling cascades are observed, as is normal near quasiperiodic behaviour. The interchange between locking and quasiperiodic behaviour persists until we approach the homoclinic wedge at negative values of ϵ_2.

As this homoclinic wedge is approached, apparently chaotic dynamics is observed, consistent with the appearance of horseshoes associated with the im-

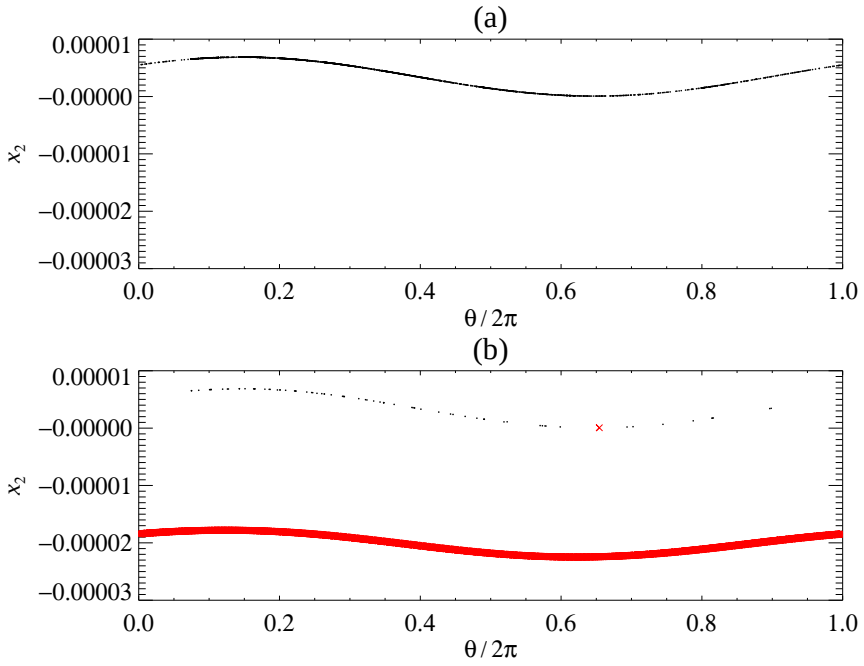

Figure 9. Illustration of how leaking develops as the attractor crosses $\mathcal{W}^{\mathrm{s}}(P)$ (approximately $x_2 = 0$ in this figure). (a) Poincaré map for the orbit shown in figure 8(a); (b) Poincaré map for the orbit in figure 8(b). In each case the Poincaré section is H_1^{in} with $|x_3| = h = 0.005$. In each panel, a dot (resp. cross) indicates that the orbit next crosses the Poincaré section with $x_2 > 0$ (resp. $x_2 < 0$). In (b), the upper collection of dots corresponds to the chaotic transient, which ends in a single cross, after which the orbit switches to a quasiperiodic attractor, represented by the lower collection of crosses.

pending homoclinic tangency. Before the first tangency is reached (labelled B in figure 4), orbits are trapped in the region with $x_2 > 0$, $x_3 > 0$ (figure 8a). If ϵ_2 is decreased past the tangency value (labelled C), the attractor crosses $\mathcal{W}^{\mathrm{s}}(P)$ and so a typical orbit will display a chaotic transient with $x_2 > 0$, $x_3 > 0$, and then switch to $x_2 < 0$, $x_3 > 0$, after which the orbit is attracted to a quasiperiodic solution in that quarter of phase space (figure 8b). Corresponding Poincaré maps are shown in figure 9. With negative values of ϵ_2, once the trajectory has switched to $x_2 < 0$, the behaviour is analogous to that observed with $\epsilon_2 > 0$ and $x_2 > 0$: quasiperiodic attractors interspersed with frequency locking. Note there is no persistent switching in x_2, and no switching in x_3, for these parameter values.

If ϵ_2 is now increased from $\epsilon_2 = 3 \times 10^{-5}$ while ϵ_1 and ϵ_3 are kept fixed as before, we approach the wedge of heteroclinic connections from $-E_3$ to $+E_2$

(following the dotted line in figure 4). Once the left edge of the heteroclinic wedge has been crossed, orbits can switch from $x_3 < 0$ to $x_3 > 0$ (but not from $x_3 > 0$ to $x_3 < 0$). For example, at $\epsilon_2 = 1.1 \times 10^{-4}$ (labelled D in figure 4), we find a chaotic transient with $x_3 < 0$ that has a single switch to a locked periodic orbit with $x_3 > 0$, in a manner similar to the single x_2 switch in figure 8(b). For larger ϵ_2, we find other examples of quasiperiodicity, locked periodic orbits, chaos, chaotic transients and single switches from $x_3 < 0$ to $x_3 > 0$, consistent with the analysis presented above. We did not find any examples of persistent switching.

The behaviour for negative values of ϵ_2 and/or ϵ_3 is analogous: single switches can be found, but there is no persistent switching for $\epsilon_1 = 10^{-4}$. However, persistent switching in one or both of x_2 and x_3 is observed if we increase ϵ_1. Figures 10 and 11 show an example of persistent switching in x_2 (but not x_3) for $\epsilon_1 = 3 \times 10^{-4}$, $\epsilon_2 = 2 \times 10^{-4}$ and $\epsilon_3 = 0.001$. The trajectory crosses the Poincaré section in a curve that appears reasonably smooth at the largest scale (figure 11), but the magnified inset shows that the curve has structure, and that parts of the curve lie below $\mathcal{W}^{\mathrm{s}}(P)$, leading to switches from $x_2 > 0$ to $x_2 < 0$. For these parameter values, there appears to be no attractor with $x_2 < 0$, and after a short transient, the trajectory switches back to $x_2 > 0$. Dynamics with a larger value of $\epsilon_1 = 0.005$ is shown in figures 12 and 13: here we have persistent switching in x_2 and x_3.

Our understanding of the mechanism behind persistent switching in x_2 or x_3 requires that ϵ_1 be large enough that $1 + \epsilon_1 g_3(\theta)$ or $1 + \epsilon_1 g_1(\theta)$ can take on positive and negative values, as a function of θ. In order to illustrate this effect, we have fitted these functions using the trajectories in figures 10 ($\epsilon_1 = 3 \times 10^{-4}$) and 12 ($\epsilon_1 = 0.005$). We have concentrated on switching in x_3, so the fact that these trajectories are for different values of ϵ_2 does not affect our conclusions. We took the coordinates (x_3, θ_1) on the section H_1^{out} and $\tilde{x}_3$ from the next intersection with H_2^{in}, and used these data to fit a map of the form of Ψ_{12}:

$$\tilde{x}_3 = x_3 \left(A_1 + \epsilon_1 f_1(\theta_1)\right) + \epsilon_3 \left(1 + \epsilon_1 g_1(\theta_1)\right),$$

see equation (18). We represented the two functions f_1 and g_1 by a finite Fourier series, and were able to fit the data to within one part in 1000 for all points with the smaller value of ϵ_1, and to within one part in 100 for all but

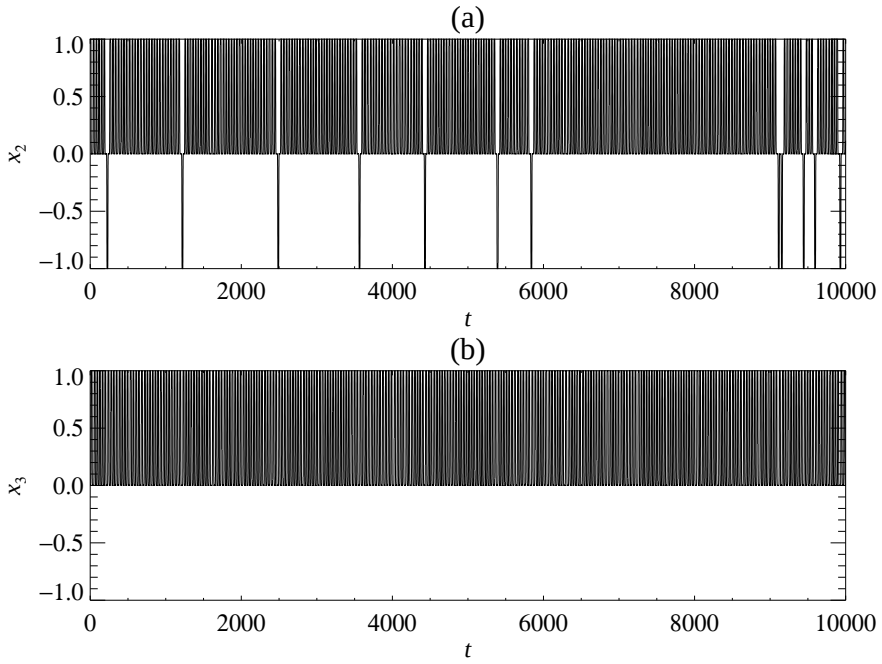

Figure 10. Time series showing persistent switching in x_2 alone, for equations (10–12) with $\epsilon_1 = 3 \times 10^{-4}$, $\epsilon_2 = 2 \times 10^{-4}$, $\epsilon_3 = 0.001$. The other coefficients are as defined in text.

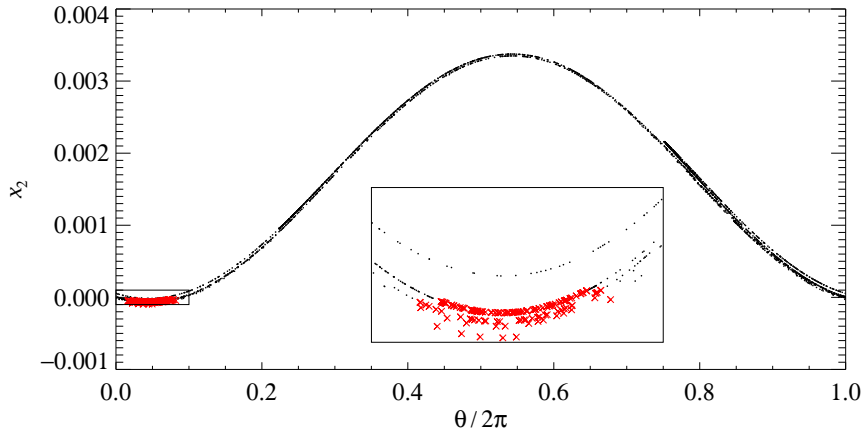

Figure 11. Poincaré section corresponding to the time series shown in figure 10. The inset shows an enlargement of the region in the box marked in the main picture. The Poincaré section is H_1^{in} with $|x_3| = h = 0.01$. A dot (resp. cross) indicates that the orbit next crosses the Poincaré section with $x_2 > 0$ (resp. $x_2 < 0$). The inset shows that crosses (indicating a switch) occur where the trajectory lies below $\mathcal{W}^{\text{S}}(P)$ (approximately $x_2 = 0$).

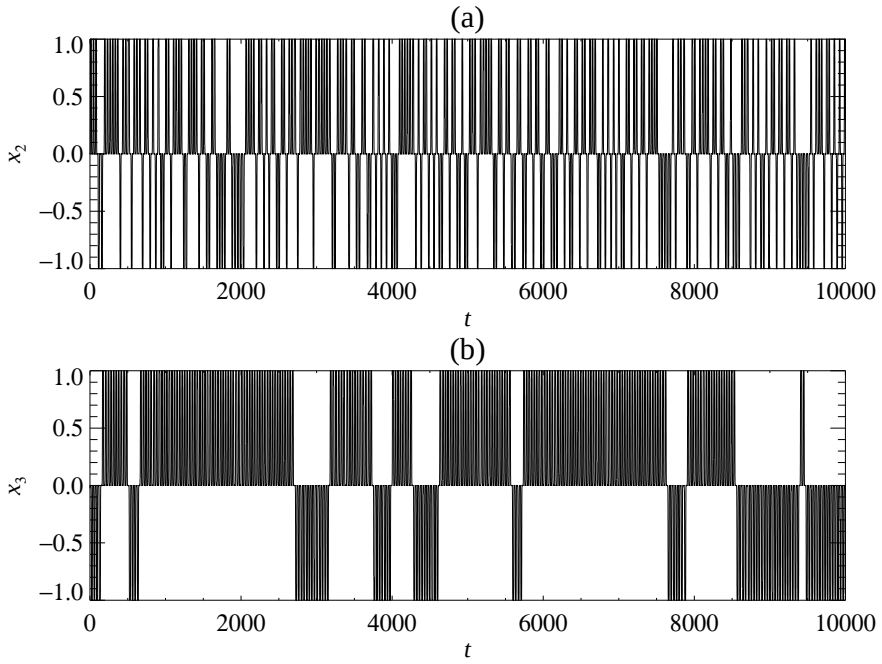

Figure 12. Time series showing persistent switching in x_2 and x_3, for (10–12) with $\epsilon_1 = 0.005$, $\epsilon_2 = 3 \times 10^{-5}$, $\epsilon_3 = 0.001$. Other coefficients as defined in text.

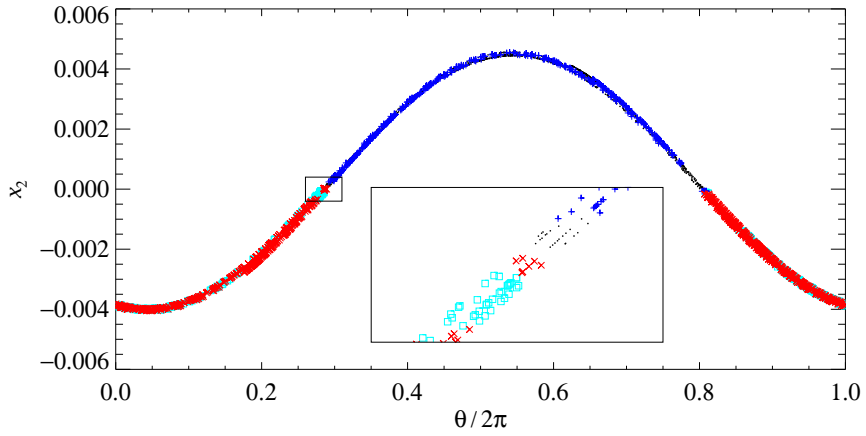

Figure 13. Poincaré section corresponding to the time series shown in figure 12. The inset shows an enlargement of the region in the box marked in the main picture. The Poincaré section is $H_1^{\rm in}$ with $|x_3| = h = 0.01$. Four symbols are used: a dot (resp. cross) indicates that the orbit next crosses the Poincaré section with $x_2 > 0$ (resp. $x_2 < 0$) and with $x_3 > 0$. A + (resp. square) indicates that the orbit next crosses the Poincaré section with $x_2 > 0$ (resp. $x_2 < 0$) and with $x_3 < 0$. The division between orbits falling either side of $\mathcal{W}^{\rm S}(P)$ is clearly visible. Orbits falling on opposite sides of $\mathcal{W}^{\rm S}(\pm E_2)$ are reasonably well mixed with this choice of cross-section.

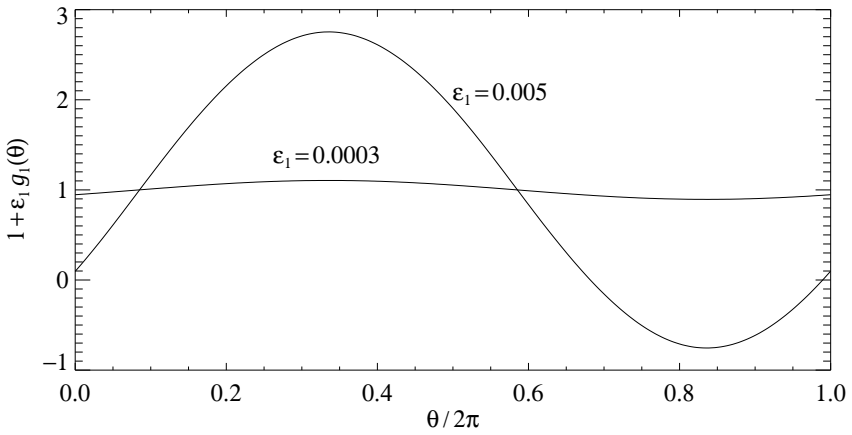

Figure 14. The function $1 + \epsilon_1 g_1(\theta)$ fitted to the data in figures 10 ($\epsilon_1 = 3 \times 10^{-4}$) and 12 ($\epsilon_1 = 0.005$). This function must be both positive and negative as a function of θ in order to allow persistent switching in x_3.

a handful of the points for the larger value of ϵ_1. As expected, the $A_1 + \epsilon_1 f_1$ part of the map remains positive, but $1 + \epsilon_1 g_1$ can change sign for the larger value of ϵ_1, as shown in figure 14. Indeed, the numerical ratio of the amplitudes of the two fitted functions is 16.663 while the ratio of the two values of ϵ_1 is 16.667. Our understanding requires the change in sign of $1+\epsilon_1 g_1$ as a necessary condition for persistent switching in x_3, which is confirmed by this illustration and by our other calculations. A similar transition occurs (at a smaller value of ϵ_1) at the onset of persistent switching in x_2, and in that case, the data can be fitted to within 1 part in 10,000 or better.

We note that we were able to find parameter values associated with persistent switching in x_2 alone but were unable to get persistent switching in x_3 without also having switching in x_2. This is a consequence of the particular choice of symmetry-breaking coefficients we use: the threshold in ϵ_1 for persistent switching in x_3 is higher than the threshold for persistent switching in x_2 for the chosen coefficients (since we have $d_{23} > d_{33}$). For other parameter choices, the thresholds could be the other way around.

In the numerical simulations described above, the quantities δ_1, δ_2, δ_3 and δ were all greater than one. This choice was made to ensure that that the heteroclinic cycle was attracting in the fully symmetric case and to remove any possible complications due to chaotic dynamics associated with homoclinic bifurcations of $\pm E_2$ and $\pm E_3$. Much of the same switching dynamics will still

occur if one or both of δ_2 and δ_3 is less than one while $\delta > 1$, since the mechanism for switching we have found does not depend on the size of the individual δ_i. However, in this case there may be additional complications in the dynamics associated with the homoclinic bifurcations of the equilibria.

6 Conclusions

This paper has investigated the effect of small symmetry-breaking on the dynamics near a structurally stable heteroclinic cycle connecting two equilibria and a periodic orbit. The heteroclinic cycle is structurally stable in the case that there are two reflection symmetries and a rotation symmetry in the underlying system; we were interested in the dynamics seen when one or more of the symmetries is broken. It was reported in [20] that this type of system can exhibit seemingly chaotic dynamics along with repeated but irregular switching of sign of various variables, but details of the mechanisms underlying the onset of complicated dynamics were not explored there. In this paper, we have identified global bifurcations that induce the onset of chaotic dynamics and switching near a heteroclinic cycle of this type. These turn out to be homoclinic tangencies between the stable and unstable manifolds of the periodic orbit, and specific heteroclinic tangencies between stable and unstable manifolds of the two equilibria. By construction and analysis of approximate return maps, we were able to locate (approximately) the global bifurcations in parameter space and hence to isolate instances of the different types of switching and chaotic dynamics in a specific numerical example.

In addition to identification of the mechanisms underlying the onset of switching, two important insights have been gained from this study. First, we found that interaction of the different symmetry-breaking terms is required for switching; partial symmetry breaking (where one or two of the three symmetries are retained) did not result in switching. Switching results from the right combination of a global bifurcation (which results in turn from breaking of the rotation symmetry) and small breaking of at least one of the reflection symmetries. Second, we found there is a threshold in ϵ_1 below which there can be single switches in the signs of certain variables but no persistent switching. The important point here is that persistent switching does not result from arbitrarily small symmetry breaking, but is a 'large' symmetry-breaking effect.

Of course, 'small' and 'large' are relative terms, and addition of seemingly tiny symmetry-breaking effects might actually result in persistent switching, as was the case in the numerical example we investigated in section 5.

One aspect of this problem which has not yet been investigated is whether it is possible to make *a priori* predictions about switching rates or derive scaling laws for switching times. It is plausible that switching rates and times might depend on the 'distance' from the global bifurcation that induces the switching, but no detailed attempts have yet been made to quantify such a relationship. The statistics of switching intervals were measured in the related model of [20], who report an exponential distribution of intervals between switches.

Finally, we note that the dynamo model in [20] has a symmetry that is never broken (this is the symmetry $(z_1, x_2, x_3) \to (-z_1, -x_2, -x_3)$ in the notation of [20]). Retention of this symmetry while breaking all others amounts to retaining invariance of the $z_1 = x_2 = x_3 = 0$ subspace, and will have a consequence of relating the dynamics in different parts of the phase space. For example, if it is possible to switch from $(x_2 > 0, x_3 > 0)$ to $(x_2 > 0, x_3 < 0)$, it will also be possible to switch from $(x_2 < 0, x_3 < 0)$ to $(x_2 < 0, x_3 > 0)$. Our results do not include this effect, and retaining this symmetry may well have profound effects on the switching properties. Nevertheless we expect our basic ideas about switching being induced by a balance between a global bifurcation and symmetry-breaking terms and the existence of a threshold for persistent switching to apply quite generally, and to the example in [20] in particular, even if the details turn out not to be directly relevant.

7 Appendix: Details of return map construction

7.1 *Coordinates and cross-sections*

Following [4], we distinguish radial, contracting, and expanding directions near the equilibria in the fully symmetric case. If $\mathcal{P}_1 = \{(z_1, x_2, x_3) : x_3 = 0\}$, $\mathcal{P}_2 = \{(z_1, x_2, x_3) : z_1 = 0\}$, $\mathcal{P}_3 = \{(z_1, x_2, x_3) : x_2 = 0\}$, with $\mathcal{P}_0 \equiv \mathcal{P}_3$, then the radial eigenvalues at $\pm E_j$ $(j = 2, 3)$ are the eigenvalues of the linearised vector field at $\pm E_j$ (i.e., eigenvalues of $(d\mathbf{f})_{\pm E_j}$) restricted to $\mathcal{P}_j \cap \mathcal{P}_{j-1}$. The contracting eigenvalues are the remaining eigenvalues of $(d\mathbf{f})_{\pm E_j}$ in $\mathcal{P}_{j-1}$, and the expanding eigenvalues are the remaining eigenvalues in $\mathcal{P}_j$. The ra-

dial direction is then the span of the eigenvectors corresponding to the radial eigenvalues, and similarly for the contracting and expanding directions. Near P we define the radial direction to be the direction of $\mathcal{P}_1 \cap \mathcal{P}_3$ (i.e., the plane $x_2 = x_3 = 0$), the contracting direction is parallel to the x_3-axis, and the expanding direction is parallel to the x_2-axis. These definitions are consistent with those in [4] but are adapted for the case where there is a periodic orbit in the heteroclinic cycle.

We choose local coordinates near each of P, $\pm E_2$, and $\pm E_3$ to make the linearised dynamics as simple as possible. Near $+E_2$ in the fully symmetric case, we define $\xi_2 = x_2 - \bar{x}_2$, where $\bar{x}_2$ is the value of x_2 at $+E_2$, and then use local coordinates (z_1, ξ_2, x_3); z_1, ξ_2 and x_3 correspond to the contracting, radial and expanding directions, respectively. Under symmetry breaking, $+E_2$ moves in proportion to the magnitude of the symmetry breaking, and the local coordinates are measured from the new position of the equilibrium point. The eigenvalues and eigenvectors change similarly, but since the eigenvalues are generically distinct and non-zero, small symmetry-breaking will not change the nature of the local structure and we can use the slightly altered eigenvectors to define a slightly altered local coordinate system. We continue to identify radial, contracting and expanding directions once weak symmetry breaking is introduced, in the obvious way, and retain the notation (z_1, ξ_2, x_3), for the altered coordinates, although z_1 and x_3 may no longer coincide with the corresponding global coordinates.

A similar construction is used near $-E_2$ except that $\xi_2 = -x_2 + \bar{x}_2$, where $\bar{x}_2$ is the value of x_2 at $-E_2$. The point of defining ξ_2 in this way is that positive values of ξ_2 near $+E_2$ are mapped under the reflection κ_2 to positive values of ξ_2 near $-E_2$, and this simplifies the maps we derive below. An analogous procedure is used to define local coordinates near $\pm E_3$.

To construct local coordinates near P, we select a cross-section transverse to P, say $\theta_1 = 0$. Near P, the flow induces a map from that section to itself, with P corresponding to a fixed point of the map. We define $\xi_1 = r_1 - \bar{r}_1$, where $\bar{r}_1$ is the value of r_1 at the fixed point; ξ_1 is the analogue in the map to the radial coordinate for the flow near P. The remaining local coordinates on the cross-section are defined by restricting the expanding and contracting directions at P, as defined above, to the cross-section. Local coordinates can be extended to a neighbourhood of the whole of P in the fully symmetric case by

applying equivariance under κ_1. Finally, small symmetry-breaking perturbations will not change the local structure near P, and we can extend to slightly altered local coordinates $(\xi_1, \theta_1, x_2, x_3)$ in a neighbourhood of P so long as we remember that symmetry-breaking terms may have a different effect at each value of θ_1, so for instance, $z_1 = \bar{r}_1 \mathrm{e}^{\mathrm{i}\theta_1}$ where $\bar{r}_1 \equiv r_1(\theta_1)$ is a function of θ_1. Note that the global polar coordinates (r_1, θ_1) are well-defined near P even in the presence of small symmetry breaking since P is far from the origin.

Cross-sections in $\mathbb{R}^4$ are defined in terms of local coordinates as follows:

$$\begin{aligned}
H_1^{\mathrm{in}} &= \{(\xi_1, \theta_1, x_2, x_3) : |\xi_1| \le h, 0 \le \theta_1 < 2\pi, |x_2| \le h, |x_3| = h\}, \\
H_1^{\mathrm{out}} &= \{(\xi_1, \theta_1, x_2, x_3) : |\xi_1| \le h, 0 \le \theta_1 < 2\pi, |x_2| = h, |x_3| \le h\}, \\
H_2^{\mathrm{in}} &= \{(z_1, \xi_2, x_3) : |z_1| = h, |\xi_2| \le h, |x_3| \le h\}, \\
H_2^{\mathrm{out}} &= \{(z_1, \xi_2, x_3) : |z_1| \le h, |\xi_2| \le h, |x_3| = h\}, \\
H_3^{\mathrm{in}} &= \{(z_1, x_2, \xi_3) : |z_1| \le h, |x_2| = h, |\xi_3| \le h\}, \\
H_3^{\mathrm{out}} &= \{(z_1, x_2, \xi_3) : |z_1| = h, |x_2| \le h, |\xi_3| \le h\}.
\end{aligned}$$

The cross-sections H_2^{in} and H_2^{out} (resp. H_3^{in} and H_3^{out}) work equally well near $\pm E_2$ (resp. $\pm E_3$) so long as the local coordinate ξ_2 (resp. ξ_3) is interpreted correctly, as described above.

We also define a Poincaré section for the periodic orbit P:

$$H_1^P = \{(\xi_1, \theta_1, x_2, x_3) : |\xi_1| \le h, \theta_1 = 0, |x_2| \le h, |x_3| \le h\}.$$

Trajectories visiting P first cross H_1^{in}, may then cross H_1^P several times, and eventually leave the neighbourhood of P on crossing H_1^{out}.

7.2 *Local maps*

Within a neighbourhood of each of $\pm E_2$, $\pm E_3$ and P, so long as certain non-resonance conditions on the eigenvalues are satisfied, the dynamics can be linearised using the Hartman–Grobman theorem [37]. In the fully symmetric case, the dynamics near P can be approximated by:

$$\dot{\xi}_1 = -2\xi, \qquad \dot{\theta}_1 = 1, \qquad \dot{x}_2 = e_1 x_2, \qquad \dot{x}_3 = -c_1 x_3,$$

where e_1 and c_1 are positive constants. Without loss of generality, we have assumed that the radial eigenvalue is -2, and that the angular speed is 1. Solving these equations, we find the local map $\phi_1 : H_1^{\rm in} \to H_1^{\rm out}$ is given by:

$$\phi_1(\xi_1, \theta_1, x_2, x_3) = \left(\xi_1 \left|\frac{x_2}{h}\right|^{\gamma_1}, \theta_1 - \frac{1}{e_1} \ln \left|\frac{x_2}{h}\right|, h\,\mathrm{sgn}(x_2), h\,\mathrm{sgn}(x_3) \left|\frac{x_2}{h}\right|^{\delta_1} \right), \tag{13}$$

where the initial value of x_3 satisfies $|x_3| = h$, where $\mathrm{sgn}(x) = +1$ if $x > 0$, $\mathrm{sgn}(x) = -1$ if $x < 0$, and $\mathrm{sgn}(0) = 0$, and where $\delta_1 = c_1/e_1$, $\gamma_1 = 2/e_1$.

The argument that symmetry-breaking does not affect this local map goes as follows. The transition from $H_1^{\rm in} \to H_1^{\rm out}$ has three parts. First, the trajectory travels from $H_1^{\rm in} \to H_1^P$ in less than one circuit around P. The trajectory does not get very close to P in this time, having started at least a distance h from it. Since the ϵ_i's, which control the symmetry breaking, are assumed to be much smaller than h, the fully symmetric flow yields an adequate approximation of the true flow. Second, the trajectory makes n_1 circuits around the periodic orbit from H_1^P to H_1^P, where n_1 is a non-negative integer no greater than $T_1/2\pi$. These circuits are governed by the linearised Poincaré map and its Floquet multipliers: $\mathrm{e}^{-4\pi}$, $\mathrm{e}^{2\pi e_1}$ and $\mathrm{e}^{-2\pi c_1}$ in the radial, expanding and contracting directions, respectively, where, to leading order in the ϵ_i's, the period of P is 2π. The number n_1 is unchanged by the weakly broken symmetry, and so, to leading order, this part of the map is unchanged. Third, the trajectory travels from $H_1^P \to H_1^{\rm out}$ in less than one circuit around P and again is not too close to P, so the fully symmetric flow yields an adequate approximate of the true flow. Composing these three parts yields (13), to leading order.

Local maps $\phi_2 : H_2^{\rm in} \to H_2^{\rm out}$ and $\phi_3 : H_3^{\rm in} \to H_3^{\rm out}$ are obtained similarly:

$$\phi_2(r_1 = h, \theta_1, \xi_2, x_3) = \left(h \left|\frac{x_3}{h}\right|^{\delta_2}, \theta_1 - \frac{1}{e_2} \ln \left|\frac{x_3}{h}\right|, \xi_2 \left|\frac{x_3}{h}\right|^{\gamma_2}, h\,\mathrm{sgn}(x_3) \right), \tag{14}$$

$$\phi_3(r_1, \theta_1, x_2, \xi_3) = \left(h, \theta_1 - \frac{1}{e_3} \ln \left(\frac{r_1}{h}\right), h\,\mathrm{sgn}(x_2) \left(\frac{r_1}{h}\right)^{\delta_3}, \xi_3 \left(\frac{r_1}{h}\right)^{\gamma_3} \right), \tag{15}$$

where c_i and e_i are the absolute values of the real part of the contracting and expanding eigenvalues at $+E_i$, $\delta_i = c_i/e_i$, $\gamma_i = 2/e_i$, and $|x_2| = h$. As for ϕ_1, the radial eigenvalues and the angular speeds are chosen to be -2 and 1.

7.3 *Global maps*

The global map $\Psi_{12} : H_1^{\rm out} \to H_2^{\rm in}$ takes orbits from a neighbourhood of P to a neighbourhood of $+E_2$. We write

$$\Psi_{12}(\xi_1, \theta_1, x_2 = h, x_3) = (\tilde{r}_1 = h, \tilde{\theta}_1, \tilde{\xi}_2, \tilde{x}_3)$$

and initially do not include symmetry-breaking effects. The unstable manifold of P is two-dimensional and, locally, intersects $H_1^{\rm out}$ at

$$\mathcal{W}^{\rm u}(P) \cap H_1^{\rm out} = \{(\xi_1, \theta_1, x_2, x_3) : \xi_1 = 0, 0 \le \theta_1 < 2\pi, x_2 = \pm h, x_3 = 0\} \quad (16)$$

The manifold $\mathcal{W}^{\rm u}(P)$ has two branches: the *positive* branch intersects $H_1^{\rm out}$ with $x_2 = h$ and the *negative* branch intersects $H_1^{\rm out}$ with $x_2 = -h$. The positive branch forms a connection from P to $+E_2$ and is the solution we now linearise about, while the negative branch forms a connection from P to $-E_2$ and will be discussed later. The positive branch of $\mathcal{W}^{\rm u}(P)$ intersects $H_2^{\rm in}$ at

$$\left\{(r_1, \theta_1, \xi_2, x_3) : r_1 = h, 0 \le \theta_1 < 2\pi, \xi_2 = \bar{\xi}_2, x_3 = 0\right\} \quad (17)$$

where $\bar{\xi}_2$ is a small constant. The κ_1 symmetry forces the heteroclinic orbit corresponding to the choice θ_1 in (16) to have an angular component in $H_2^{\rm in}$ of $\theta_1 + \bar{\theta}_1$ for some constant $\bar{\theta}_1$, i.e., the global map acts on the angle as a rigid rotation. Furthermore, trajectories that are near but not on the unstable manifold of $\mathcal{W}^{\rm u}(P)$ have $\tilde{\xi}_2$ and $\tilde{x}_3$ depending on the initial ξ_1 and x_3 but not on θ_1, while $\tilde{\theta}_1 = \theta_1 + \bar{\theta}_1$ where $\bar{\theta}_1$ is a function of the initial ξ_1 and x_3. Equivariance under κ_3 ensures that the subspace $x_3 = 0$ is invariant, that $\tilde{x}_3$ is an odd function of x_3, and that $\bar{\theta}_1$ and $\tilde{\xi}_2$ are even functions of x_3. (The κ_2 symmetry has no role in determining the form of Ψ_{12} although it can be used to construct a map from P to $-E_2$ once Ψ_{12} is known.) Writing a Taylor series in the small quantities ξ_1 and x_3 therefore yields

$$\begin{aligned}
\tilde{\theta}_1(\xi_1, \theta_1, x_3) = \theta_1 + \bar{\theta}_1(\xi_1, x_3) &= \theta_1 + \bar{\theta}_1(0,0) + \text{h.o.t.}, \\
\tilde{\xi}_2(\xi_1, x_3) &= \tilde{\xi}_2(0,0) + \text{h.o.t.}, \\
\tilde{x}_3(\xi_1, x_3) &= \frac{\partial \tilde{x}_3}{\partial x_3}(0,0)\, x_3 + \text{h.o.t.},
\end{aligned}$$

where h.o.t. denotes higher order terms. Effectively, so long as $\bar{\theta}_1$ and $\tilde{\xi}_2$ are non-zero, they can be replaced by constants, while $\tilde{x}_3$ depends linearly on x_3. We write $A_1 = \frac{\partial \tilde{x}_3}{\partial x_3}(0,0)$ and $B_1 = \tilde{\xi}_2(0,0)$, and note that $A_1 > 0$ since the region of phase space with $x_3 > 0$ is dynamically invariant.

The effect of weak symmetry breaking on these expressions is as follows. First, the symmetry $x_3 \to -x_3$ is broken by including terms that are odd in x_3 in the expressions for $\tilde{\theta}_1$ and $\tilde{\xi}_2$, and terms that are even in x_3 in the expression for $\tilde{x}_3$. We multiply all such terms by an overall factor of ϵ_3, which is a real constant that controls the magnitude of the breaking of the κ_3 symmetry. Then the lowest order contribution to $\tilde{\theta}_1$ and $\tilde{\xi}_2$ will be a term in $\epsilon_3 x_3$ while $\tilde{x}_3$ will pick up a term linear in ϵ_3. At leading order all quadratic terms can be dropped, so the only new term is one linear in ϵ_3 in the expression for $\tilde{x}_3$. Second, breaking the κ_1 symmetry will result in a weak dependence of all the coefficients on θ_1, with the dependence being periodic in that variable. We introduce the parameter ϵ_1, which is a real constant that multiplies all terms that break the κ_1 symmetry and that controls the magnitude of the symmetry-breaking terms. For example, A_1 will become $A_1 + \epsilon_1 f_1(\theta)$, with the caveat that this term must remain positive, for all θ and ϵ_1. Third, weakly breaking the symmetry $x_2 \to -x_2$ will not affect the form of this map.

Putting all this together results in a map $\Psi_{12} : H_1^{\text{out}} \to H_2^{\text{in}}$:

$$\Psi_{12}(\xi_1, \theta_1, x_2 = h, x_3) = \big(\tilde{r}_1 = h, \tilde{\theta}_1 = \theta_1 + \Phi_1, \tilde{\xi}_2 = B_1, \\ \tilde{x}_3 = A_1 x_3 + \epsilon_3 + \epsilon_1 x_3 f_1(\theta_1) + \epsilon_1 \epsilon_3 g_1(\theta_1)\big), \quad (18)$$

where Φ_1, A_1, B_1 are constants, and f_1, g_1 are 2π-periodic functions of θ_1. The θ_1 dependence cannot be treated using Taylor series expansions, as θ_1 is not a small quantity. We explain below why some quadratic terms ($\epsilon_1 x_3$ and $\epsilon_1 \epsilon_3$) need to be kept.

Similarly, a map from P to $-E_2$ can be constructed. This has precisely the form of (18), except that it starts from $x_2 = -h$. Breaking of the κ_2 symmetry means coefficients in the map will be slightly different but the map is unchanged at leading order.

The map $\Psi_{23} : H_2^{\text{out}} \to H_3^{\text{in}}$ is calculated in a similar way. In the fully symmetric case, we linearise about $\mathcal{W}^{\text{u}}(+E_2)$, which intersects H_2^{out} at $(z_1 = 0, \xi_2 = 0, x_3 = h)$ and H_3^{in} at $(z_1 = 0, \xi_2 = h, \xi_3 = \bar{\xi}_3)$ where $\bar{\xi}_3$ is a small

constant. For orbits near $\mathcal{W}^{\mathrm{u}}(+E_2)$, the value of ξ_2 at H_2^{out} does not influence the final position to leading order and z_1 at H_3^{in} depends linearly on the values of z_1 at H_2^{out}: $\tilde{z}_1 = A_2 \mathrm{e}^{\mathrm{i}\Phi_2} z_1$ for real constants $A_2 > 0$, Φ_2. If the κ_1 symmetry is broken, $\mathcal{W}^{\mathrm{u}}(+E_2)$ leaves H_2^{out} with $z_1 = 0$ and arrives at H_3^{in} with $z_1 = \tilde{\epsilon}_1$, where $\tilde{\epsilon}_1 = \epsilon_1(a_{\mathrm{r}} + \mathrm{i}a_{\mathrm{i}})$ for a_{r} and a_{i} real constants and ϵ_1 as defined earlier. Writing the resulting map in terms of the real and imaginary parts of $\tilde{z}_1$:

$$\begin{aligned}\Psi_{23}(r_1, \theta_1, \xi_2, x_3 = h) = \big(&\tilde{x}_1 = \epsilon_1 a_{\mathrm{r}} + A_2 r_1 \cos(\theta_1 + \Phi_2),\\ &\tilde{y}_1 = \epsilon_1 a_{\mathrm{i}} + A_2 r_1 \sin(\theta_1 + \Phi_2),\\ &\tilde{x}_2 = h, \tilde{\xi}_3 = B_2\big),\end{aligned} \tag{19}$$

where a_{r}, a_{i}, A_2, B_2 and Φ_2 are real constants determined by the global flow, and $A_2 > 0$. As in Ψ_{12}, there are 2π-periodic functions of θ_1 in the map, but here the functions are known explicitly because the z_1 variable is small throughout the transition from $+E_2$ to $+E_3$, and the dynamics of z_1 is well-approximated by a scaled rotation. Similar maps can be obtained for the three connections $-E_2 \to +E_3$ and $\pm E_2 \to -E_3$; although the coefficients will be slightly different in each case, to lowest order we obtain the same map for each of the other connections so long as the signs of the x_3 (resp. $\tilde{x}_2$) components are chosen appropriately on the incoming (resp. outgoing) cross-sections (for example, the map from $-E_2$ to $-E_3$ will have $x_3 = -h$ and $\tilde{x}_2 = -h$).

The global map $\Psi_{31} : H_3^{\mathrm{out}} \to H_1^{\mathrm{in}}$ is calculated in a similar way:

$$\begin{aligned}\Psi_{31}(r_1 = h, \theta_1, x_2, \xi_3) = \big(&\tilde{\xi}_1 = B_3, \tilde{\theta}_1 = \theta_1 + \Phi_3,\\ &\tilde{x}_2 = A_3 x_2 + \epsilon_2 + \epsilon_1 x_2 f_3(\theta_1) + \epsilon_1\epsilon_2 g_3(\theta_1),\\ &\tilde{x}_3 = h\big),\end{aligned} \tag{20}$$

where A_3, B_3 and Φ_3 are real constants, f_3 and g_3 are 2π-periodic functions of θ_1, and ϵ_1 controls the size of the terms that break the κ_1 symmetry. The parameter ϵ_2 introduced in (20) is analogous to ϵ_3, and is a real quantity that controls the size of all terms that break the κ_2 symmetry. Similarly to the case for A_1 argued above, we take $A_3 + \epsilon_1 f_3(\theta_1)$ to be positive for all values of ϵ_1. A similar map can be defined near the connections from $-E_3$ to P, and will, to leading order, be identical to (20) so long as $\tilde{x}_3 = h$ is replaced by $\tilde{x}_3 = -h$.

The effect of each of the global maps defined above is, at leading order, to rotate the angular variable by an order one amount that is independent of other variables, to set the radial variable to a constant, and, in the absence of symmetry-breaking, to scale the variable that measures proximity to the cycle. Symmetry-breaking enters in two ways. First, it destroys the invariant subspaces thus destroying some of the heteroclinic connections that made up the cycle. Second, breaking the κ_1 rotation symmetry allows θ_1 dependence to enter into the maps, most importantly through the variables x_3 in the Ψ_{12} map and x_2 in the Ψ_{31} map. It is this θ_1 dependence that allows the heteroclinic tangencies discussed in Section 2.

7.4 *Return maps*

Return maps approximating the dynamics near the heteroclinic cycle can now be computed by composing the local and global maps in an appropriate order. For instance, to obtain the various forms of the map $R : H_3^{\rm in} \to H_3^{\rm in}$ given by equations (1–5) we calculate $R \equiv \psi_{23} \circ \phi_2 \circ \psi_{12} \circ \phi_1 \circ \psi_{31} \circ \phi_3$ in the usual way.

Acknowledgments

We thank Ian Melbourne, Edgar Knobloch and Jeff Porter for helpful conversations. This research has been supported by grants from New Zealand Institute for Mathematics and its Applications, University of Auckland Research Council, London Mathematical Society and the Engineering and Physical Sciences Research Council.

References

[1] Field, M., 1980, Equivariant dynamical systems. *Trans. Am. Math. Soc.*, **259**, 185–205.
[2] Guckenheimer, J. and Holmes, P., 1988, Structurally stable heteroclinic cycles. *Math. Proc. Camb. Phil. Soc.*, **103**, 189–192.
[3] Melbourne, I., 1991, An example of a non-asymptotically stable attractor. *Nonlinearity*, **4**, 835–844.
[4] Krupa, M. and Melbourne, I., 1995, Asymptotic stability of heteroclinic cycles in systems with symmetry. *Ergod. Th. & Dynam. Sys.*, **15**, 121–147.
[5] Krupa, M. and Melbourne, I., 2004, Asymptotic stability of heteroclinic cycles in systems with symmetry, II. *Proc. Roy. Soc. Edinburgh A*, **134**, 1177–1197.
[6] Kirk, V. and Silber, M., 1994, A competition between heteroclinic cycles. *Nonlinearity*, **7**, 1605–1621.

[7] Ashwin, P. and Chossat, P., 1998, Attractors for robust heteroclinic cycles with continua of connections. *J. Nonlinear Sci.*, **8**, 103–129.
[8] Aguiar, M., Castro, S. and Labouriau, I., 2005, Dynamics near a heteroclinic network. *Nonlinearity*, **18**, 391–414.
[9] Postlethwaite, C.M. and Dawes, J.H.P., 2005, Regular and irregular cycling near a heteroclinic network. *Nonlinearity*, **18**, 1477–1509.
[10] Scheel, A. and Chossat, P., 1992, Bifurcation d'orbites périodiques à partir d'un cycle homoclinic symétrique. *C. R. Acad. Sci. Paris*, **341**, 49–54.
[11] Chossat, P., Krupa, M., Melbourne, I. and Scheel, A., 1997, Transverse bifurcations of heteroclinic cycles in symmetric systems. *Physica D*, **100**, 85–100.
[12] Postlethwaite, C.M. and Dawes, J.H.P., 2006, A codimension-two resonant bifurcation from a heteroclinic cycle with complex eigenvalues. *Dyn. Syst. Int. J.*, **21**, 313–336.
[13] Busse, F.H. and Heikes, K.E., 1980, Convection in a rotating layer – simple case of turbulence. *Science*, **208**, 173–175, 1980.
[14] Proctor, M.R.E. and Jones, C.A., 1988, The interaction of two spatially resonant patterns in thermal convection. I. Exact 1:2 resonance. *J. Fluid Mech.*, **188**, 301–335.
[15] Nore, C., Tuckerman, L.S., Daube, O., and Xin, S., 2003, The 1:2 mode interaction in exactly counter-rotating von Kármán swirling flow. *J. Fluid Mech.*, **477**, 51-88.
[16] Armbruster, D., Guckenheimer, J., Holmes, P., 1988, Heteroclinic cycles and modulated travelling waves in systems with $O(2)$ symmetry. *Physica D*, **29**, 257–282.
[17] Melbourne, I., 1989, Intermittency as a codimension three phenomenon *J. Dyn. Stab. Sys.*, **1**, 347–367.
[18] Chossat, P., 1993, Forced reflectional symmetry breaking of an $O(2)$-symmetric homoclinic cycle. *Nonlinearity*, **6**, 723–731.
[19] Sandstede, B. and Scheel, A., 1995, Forced symmetry breaking of homoclinic cycles. *Nonlinearity*, **8**, 333–365.
[20] Melbourne, I., Proctor, M.R.E. and Rucklidge, A.M., 2001, A heteroclinic model of geodynamo reversals and excursions. In: P. Chossat, D. Armbruster and I. Oprea (Eds) *Dynamo and Dynamics, a Mathematical Challenge* (Dordrecht: Kluwer), pp. 363–370.
[21] Stone, E. and Holmes, P., 1990, Random perturbations of heteroclinic attractors. *SIAM J. Appl. Math.*, **50**, 726–743.
[22] Armbruster, D., Stone, E., Kirk, V., 2003, Noisy heteroclinic networks. *Chaos*, **13**, 71–79.
[23] Nore, C., Moisy, F., and Quartier, L., 2005, Experimental observation of near-heteroclinic cycles in the von Kármán swirling flow. *Phys. Fluids*, **17**, 064103.
[24] Clune, T. and Knobloch, E., 1994, Pattern selection in three-dimensional magnetoconvection. *Physica D*, **74**, 151–176.
[25] Kirk, V., Lane, E., Silber, M., 2007, A mechanism for switching in a heteroclinic network. In preparation.
[26] Ashwin, P., Rucklidge, A.M. and Sturman, R., 2004, Two-state intermittency near a symmetric interaction of saddle-node and Hopf bifurcations: a case study from dynamo theory. *Physica D*, **194**, 30–48.
[27] Rucklidge, A.M. and Matthews, P.C., 1995, The shearing instability in magnetoconvection. In: A. Brandt and H.J.S. Fernando (Eds) *Double-Diffusive Convection* (Washington: American Geophysical Union), pp. 171–184.
[28] Matthews, P.C., Rucklidge, A.M., Weiss, N.O. and Proctor, M.R.E., 1996, The three-dimensional development of the shearing instability of convection. *Phys. Fluids*, **8**, 1350–1352.
[29] Rucklidge, A.M., 2001, Global bifurcations in the Takens–Bogdanov normal form with D_4 symmetry near the $O(2)$ limit. *Phys Lett A*, **284**, 99–111.
[30] Ashwin, P., Field, M., Rucklidge, A.M. and Sturman, R., 2003, Phase resetting effects for robust cycles between chaotic sets. *Chaos*, **13**, 973–981.

[31] Ashwin, P., Rucklidge, A.M. and Sturman, R., 2004, Cycling chaotic attractors in two models for dynamics with invariant subspaces. *Chaos*, **14**, 571–582.

[32] Rademacher, J.D.M., 2005, Homoclinic orbits near heteroclinic cycles with one equilibrium and one periodic orbit. *J. Diff. Eqns.*, **218**, 390–443.

[33] Champneys, A.R., Kirk, V., Knobloch, E., Oldeman, B., and Rademacher, J., 2007, Unfolding a tangent equilibrium-to-periodic heteroclinic cycle. In preparation.

[34] Glendinning, P. and Sparrow, C., 1984, Local and global behaviour near homoclinic orbits *J. Stat. Phys.*, **35**, 645–696.

[35] Press, W.H., Flannery, B.P., Teukolsky, S.A. and Vetterling, W.T., 1986, Numerical Recipes – the Art of Scientific Computing. Cambridge University Press, Cambridge.

[36] Parker, T.S. and Chua, L.O., 1989, Practical Numerical Algorithms for Chaotic Systems. Springer, New York.

[37] Guckenheimer, J. and Holmes, P., 1986, Nonlinear Oscillations, Dynamical Systems, and Bifurcations of Vector Fields (second edition). Springer-Verlag, New York.